ORIGINAL ARTICLE

Probabilistic assessment of SMRFs with infill masonry walls incorporating nonlinear soil-structure interaction

F. Kazemi[1] · **N. Asgarkhani[1]** · **R. Jankowski[1]**

Abstract

Infill Masonry Walls (IMWs) are used in the perimeter of a building to separate the inner and outer space. IMWs may affect the lateral behavior of buildings, while they are different from those partition walls that separate two inner spaces. This study focused on the seismic vulnerability assessment of Steel Moment-Resisting Frames (SMRFs) assuming different placement of IMWs incorporating nonlinear Soil-Structure Interaction (SSI). The aim is to explore the damage states of IMWs and use their ability for improving the vulnerability of SMRFs. For this purpose, the three, five, seven, and nine story levels (3-Story, 5-Story, 7-Story, and 9-Story) SMRFs were modeled considering four soil types. Incremental Dynamic Analyses (IDAs) were performed to determine the seismic performance limit-state capacities of SMRFs considering the Far-Fault (FF) record subset suggested by FEMA P695. To accurately model the influence of IMWs on the seismic response of SMRFs, a Tcl programming algorithm was developed to intelligently monitor the damage states of IMWs in each floor level. Results of the analysis show that assuming different placement of IMWs can significantly increase the seismic limit-state capacities of SMRFs with and without considering SSI effects. In addition, IMWs can play a crucial role to improve the seismic performances as well as the seismic collapse probability, which may be suggested for retrofitting purposes.

Keywords Infill masonry wall · Nonlinear soil-structure interaction · Seismic limit-state capacity · Seismic collapse probability · Seismic retrofit · Damage identification

1 Introduction

The Infill Masonry Walls (IMWs) have been considered as nonstructural members and were neglected in the modeling of buildings with their strength and stiffness. In addition, seismic provisions prescribed a factor to consider IMWs effects on the fundamental period of the buildings. Engineers do not consider the IMWs in their designing procedures and this may affect their models. To overcome this issue, some experimental investigations

✉ F. Kazemi
  farzin.kazemi@pg.edu.pl

[1] Faculty of Civil and Environmental Engineering, Gdańsk University of Technology, ul. Narutowicza 11/12, 80-233 Gdansk, Poland

were made to find out the effects of IMWs on the structural response (e.g. Ramos et al. 2010, Preti et al. 2012, Salmanpour et al. 2015, Carpine et al. 2021). Brodsky and Yankelevsky (Brodsky and Yankelevsky 2017) focused on the effects of IMWs in the Reinforced Concrete (RC) frame by using half-scale specimens subjected to monotonic loads. Their results showed that IMWs increased the vertical loading resistance of the frame by an amount of 280% on average, and affected the failure mode. Nicoletti et al. (Nicoletti et al. 2020) proposed a procedure to determine the stiffness of IMWs in the modeling of RC frame and validated through an experimental work based on the in-situ impact load test. Uva et al. (Uva et al. 2012) investigated the effects of IMWs for an existing RC building located in Calabria, Italy, and proposed some factors to refine the structural response. Recently, scientific studies proved that the stiffness and strength provided by IMWs should be considered in the modeling process due to their effects on the global behavior of buildings (Mohamed and Romão 2020). In addition, the interaction between nonstructural components and structural members may lead to local damages in columns of buildings (Fardis et al. 1999; Perrone et al. 2017; Merino et al. 2020).

It is worth noting that the opening dimensions, boundary condition, geometry of wall (e.g. thickness and height), out-of-plane behavior, previous damage of IMWs, and double-leaf infills can highly influence the seismic behavior of buildings. Ozturkoglu et al. (Ozturkoglu et al. 2017) noted that the position and dimensions of openings could considerably influence the lateral stiffness and nonlinear behavior of RC structures, as compared to fully infilled and bare frames. Zuo et al. (Zuo et al. 2022) performed a parametric study to take the aspect ratio and opening dimensions of IMWs into account. Single and double-leaf infills were investigated under the in-plane and out-of-plane loads (Onat et al. 2018; Mazza and Donnici 2021). Misir et al. (Misir et al. 2016) proposed Z-ties as improving method that can help the double-leaf infills to withstand high lateral deformations. Furtado et al. (Furtado et al. 2016a, 2017) performed comprehensive experimental and numerical studies on lateral behavior and the out-of-plane failure of IMWs. They concluded that openings could reduce the frequency of IMWs by 20–40%, and the axial loads of lateral columns could increase the frequency of IMWs. In addition, they showed that the width of wall support and previous damages could considerably decrease the strength capacity of IMWs, even up to 60% (Furtado et al. 2020). Some investigations were carried out to evaluate the effects of material and geometry of IMWs, effects of lateral columns stiffness on the IMWs behavior, effects of the connection between IMWs and frame, as well as mechanical characteristics of IMWs on the seismic performance of buildings (Mazza and Donnici 2021; Wararuksajja et al. 2020; Huang et al. 2021). It was confirmed that previous damages of IMWs could significantly reduce the frequency of wall up to 5% and 35% corresponding to in-plane and out-of-plane loads (Furtado et al. 2017). Therefore, this effect should be considered for seismic vulnerability assessment of structures.

Many studies were performed to investigate the seismic failure probability of structures, while the IMWs were assumed as non-structural elements and their effects on the seismic responses were neglected (e.g. see Kazemi and Jankowski 2023a, Kazemi et al. 2023). It should be noted that the IMWs could provide additional stiffness and strength that may highly affect seismic parameters such as fundamental structural period and interstory drift ratio (Gara et al. 2021). Also, IMWs showed different limit-state levels, as compared to the structural elements, which affect the overall performance of the building. Moreover, previous damages of IMWs (i.e. in-plane damages) and different workmanships can affect the performance level and collapse capacity of IMWs (Furtado et al. 2022).

Nowadays, the growing need for constructing buildings in urban areas leads to having buildings on different soil types. Although many improvements made to model buildings

with a high amount of accuracy, it is hard to take into account the effects of Soil-Structure Interaction (SSI) in the designing process. Therefore, designers used some simplified procedures proposed by seismic codes to consider the SSI effect. Many studies have been performed assuming the SSI effects on the buildings constructed in different soil types (Dutta et al. 2004; Pitilakis et al. 2008; Raychowdhury 2011; Petridis and Pitilakis 2020). Elwardany et al. (Elwardany et al. 2017, 2019) investigated the SSI effects on buildings with Steel Moment-Resisting Frames (SMRFs) with and without IMWs subjected to the earthquake-induced colliding. They concluded that SSI and IMWs could significantly alter the behavior and structural response of buildings. Recent studies focused on the seismic probabilities of collapse based on the fragility curves to assess the vulnerability of SMRFs and RC structures (Kazemi et al. 2020, 2021a, b). Some studies used finite element models to determine the fragility curves of RC structures and confirmed the key role of SSI effects in the seismic probabilities (Pitilakis et al. 2014; Karapetrou et al. 2015). In addition, Mitropoulou et al. (Mitropoulou et al. 2016) developed fragility curves for three systems of fixed-based, two-dimensional finite element for pile foundation and Winkler spring model. Approaches of modeling SSI is a fundamental principle and neglecting the soil nonlinearity may lead to an un-conservative prediction of the system response (Pecker et al. 2014). Rajeev and Tesfamariam (Rajeev and Tesfamariam 2012) investigated the nonlinearity effects of SSI and soil parameters such as cohesion, density, Poisson's ratio, and friction angle on the seismic vulnerability of RC structures using the Beam on Nonlinear Winkler Foundation (BNWF) model. Nonlinear behavior of shallow foundations may dissipate the seismic energy through soil yielding. Harden and Hutchinson (Harden and Hutchinson 2009) introduced a simulation methodology for modeling of nonlinearity of shallow foundations using BNWF, and the model was developed as a stand-alone module as a useful tool for designing purposes by Allotey and El Naggar (Allotey and Naggar 2008). Forcellini (Forcellini 2021) investigated the SSI effects on the fragility curves of the RC structures with and without IMWs and concluded that SSI effects increased the failure probability of both RC structures.

The present paper aims to investigate the effects of different placements of IMWs, and the nonlinearity effects of SSI on the seismic response of SMRFs. Due to different collapse states for IMWs and SMRFs, a Tcl programming algorithm was developed to control demand limitations during Incremental Dynamic Analysis (IDA). Therefore, it can be possible to determine the effects of IMWs on the seismic responses considering SSI effects assuming four soil types. To determine the seismic vulnerability of SMRFs, seismic limit state capacities and seismic fragility curves were plotted and the influence of assumed parameters were investigated. The results of this study can be widely used by civil engineers for design procedures or retrofitting purposes.

2 Modeling methods

2.1 Modeling of SMRFs

In this paper, buildings with three, five, seven, and nine story levels (3-Story, 5-Story, 7-Story, and 9-Story) with considering SMRFs in four outer frames were designed according to the regular plan presented in Fig. 1. In the design process, four soil types were

Fig. 1 Considered plan for modeling of SMRFs
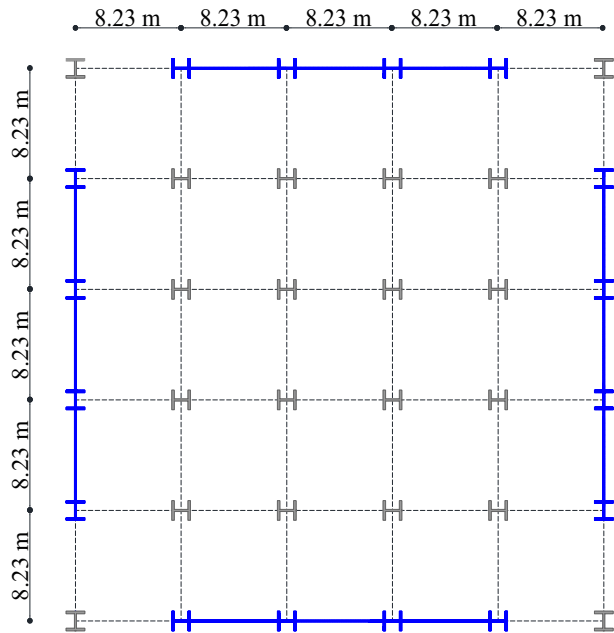
considered to model buildings located in California with a latitude of 34.039° and longitude of − 118.324°.

Table 1 presents values of the soil parameters and seismic design parameters for selected soil types. These quantities are available both in ASCE 7–16 (ASCE 2017) and on the USGS website (USGS 2022). S_{DS} and S_{D1} are numeric seismic design values at 0.2 and 1.0 s, respectively, G_0 is the initial soil shear modulus, Φ, c, γ, V_s, v are friction angle, cohesion coefficient, unit weight, shear wave velocity, and Poisson's ratio, respectively. According to the seismic force-resisting system selected for the buildings, design parameters of R, Ω_0 and C_d equal to 8, 3, and 5.5, respectively, were selected (see Table 12.2.1 ASCE 7–16 (ASCE 2017)). It is worth noting that the force-based design approach was used for designing SMRFs assuming spectral acceleration presented in Table 1 for considered soil types and provisions of ASCE 7–16 (ASCE 2017), AISC 360–16 (AISC 2016), and AISC 341–16 (see Section E3) (AISC 2016). To model three-dimensional buildings

Table 1 Soil and seismic design parameters

Soil	B	C	D	E
S_{DS}	1.306	1.567	1.576	1.623
S_{D1}	0.463	0.648	0.653	0.659
G_0 (MPa)	6000	280	60	30
Φ (Degree)	45	42	38	35
c (kPa)	0	0	5	5
γ (kN/m^3)	24	21	19	18
v	0.25	0.35	0.4	0.45
V_s (m/s)	1565	360	175	120

using ETABS 2016 software, the floor dead and live loads of 3.35 kN/m² and 1.68 kN/m² were applied, respectively. For designing the SMRFs, the parameters of $F_y = 345$ MPa (yield strength), E = 200 GPa, and $\upsilon = 0.3$ were considered for steel, and the compressive strength of concrete for designing the foundation was considered equal to 30 MPa (Kazemi et al. 2021a).

Some studies used 2D structural models in Opensees (McKenna et al. 2016) for 3D buildings (e.g. see (Kazemi et al. 2018, 2020, 2021a, b; Mohebi et al. 2018; Asgarkhani et al. 2020; Yakhchalian et al. 2020, 2021)) since the regular plan of building can allow us to neglect the torsional effects. Regarding the improvements of analytical tools in Opensees (McKenna et al. 2016), it is possible to model the deterioration effects of strength and stiffness that are suitable for 2D modeling (Ibarra et al. 2005). In this study, the 2D models were verified with 3D buildings that were modeled in ETABS 2016 software. To reduce the complexity of models, 2D models were used (instead of 3D ones) and SSI effects were added to them. According to the plan, to model SMRFs in Opensees (McKenna et al. 2016), all columns, except for those in SMRF (blue colour), were assumed as leaning columns to consider the crucial role of the P-delta effects in seismic performance (Kazemi et al. 2018; Mohebi et al. 2018; Asgarkhani et al. 2020; Yakhchalian et al. 2020, 2021). All structural elements were modelled with an elastic beam-column element with two nonlinear rotational springs according to the Modified Ibarra–Krawinkler bilinear hysteretic model (IMK Hinge) (Ibarra et al. 2005; Kazemi and Jankowski 2023b; Mohebi et al. 2021; Yazdanpanah et al. 2022). Table 2 presents the design documentation for the assumed SMRFs considering four types of soil. The region of beam-to-column connection, that is known as panel zone, was modeled to capture the deformations. To model the panel zone, the procedure introduced in Opensees (McKenna et al. 2016) was used assuming eight rigid elements and one zero-length element with a trilinear backbone curve proposed by Gupta and Krawinkler (Gupta and Krawinkler 1999).

2.2 SSI modeling

The BNWF model, which can be widely used for modeling shallow foundations, retaining walls, and piles, have the degrading hysteretic behavior with the ability of defining rules. This model employs a series of nonlinear springs and dashpots in parallel to model soil beneath the foundation. Figure 2 presents the BNWF model and implementation of the springs and dashpots. The kind of springs used in this model plays a crucial role in soil responses. Therefore, three types of springs known as the q–z spring, p–x spring, and t–x spring were used to capture the vertical and rotational resistance, and the sliding and passive resistance of the foundation, respectively. Normalized load-normalized displacement curves of these springs were plotted in Fig. 3. The BNWF model was modeled in Opensees (McKenna et al. 2016) using material models of *QzSimple* for q–z spring, *PxSimple* for p–x spring, and *TxSimple* for t–x spring (Raychowdhury 2011; Rajeev and Tesfamariam 2012; Harden and Hutchinson 2009; Raychowdhury and Hutchinson 2009; Kazemi and Jankowski 2023b)

The BNWF consists of structural beam elements between foundation and soil nodes, and soil springs defined with zero-length element (Fig. 2). To define the BNWF model parameters, the foundation of the 3-Story, 5-Story, 7-Story, and 9-Story SMRFs were designed according to the soil parameters presented in Table 1 using SAFE 2016 software. It should be added that the dimensions of foundations were controlled based on the

Table 2 Design documentation of SMRFs for soil types

| SMRF	Floor	Soil B		Soil C		Soil D		Soil E	
		Column	Beam	Column	Beam	Column	Beam	Column	Beam
3-story	1st	W14X132	W24X68	W14X159	W24X94	W14X159	W24X94	W14X159	W24X94
	2nd	W14X120	W21X68	W14X120	W24X84	W14X120	W24X94	W14X120	W24X94
	3rd	W14X120	W18X46	W14X120	W18X50	W14X120	W18X50	W14X120	W18X55
5-story	1st	W14X145	W24X76	W14X159	W24X94	W14X159	W27X102	W14X159	W27X102
	2nd	W14X120	W24X76	W14X132	W24X94	W14X132	W27X102	W14X159	W27X102
	3rd	W14X120	W24X76	W14X120	W24X84	W14X120	W24X84	W14X120	W24X84
	4th	W14X120	W24X55	W14X120	W24X84	W14X120	W24X84	W14X120	W24X84
	5th	W14X120	W24X55	W14X120	W24X55	W14X120	W24X55	W14X120	W24X55
7-story	1st	W14X145	W24X84	W14X176	W27X102	W14X176	W27X102	W14X176	W27X102
	2nd	W14X145	W24X84	W14X159	W27X102	W14X159	W27X102	W14X159	W27X102
	3rd	W14X145	W24X84	W14X145	W27X94	W14X145	W27X102	W14X145	W27X102
	4th	W14X120	W24X84	W14X120	W27X94	W14X120	W27X94	W14X145	W24X84
	5th	W14X120	W24X68	W14X120	W24X84	W14X120	W24X84	W14X120	W24X84
	6th	W14X120	W21X50	W14X120	W21X68	W14X120	W21X68	W14X120	W21X68
	7th	W14X120	W21X50	W14X120	W21X50	W14X120	W21X50	W14X120	W21X50
9-story	1st	W14X233	W27X94	W14X233	W27X114	W14X233	W27X114	W14X233	W27X114
	2nd	W14X233	W27X94	W14X233	W27X114	W14X233	W27X114	W14X233	W27X114
	3rd	W14X176	W27X94	W14X176	W27X114	W14X176	W27X114	W14X233	W27X114
	4th	W14X176	W24X94	W14X176	W27X102	W14X176	W27X102	W14X176	W27X114
	5th	W14X176	W24X94	W14X176	W27X102	W14X176	W27X102	W14X176	W27X114
	6th	W14X120	W24X84	W14X120	W24X84	W14X159	W27X94	W14X120	W27X94
	7th	W14X120	W24X84	W14X120	W24X84	W14X120	W24X84	W14X120	W24X84
	8th	W14X120	W21X50	W14X120	W21X68	W14X120	W21X68	W14X120	W24X84
	9th	W14X120	W21X50	W14X120	W21X50	W14X120	W21X50	W14X120	W21X50
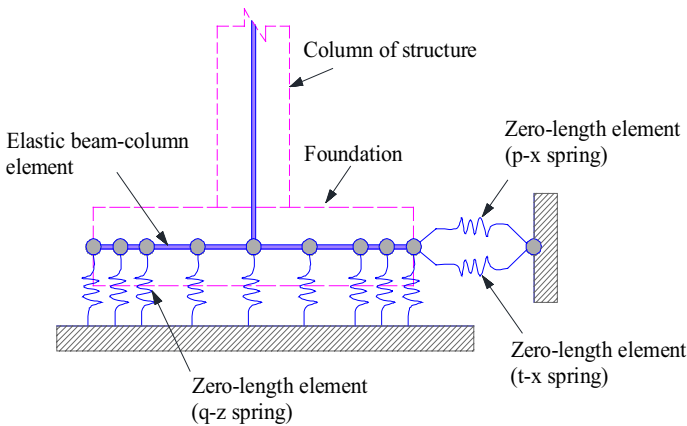
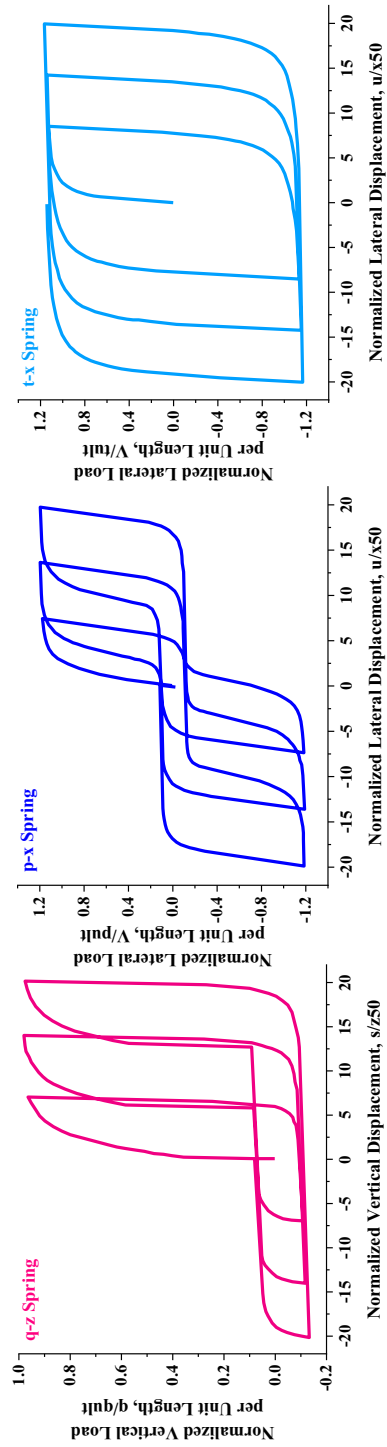**Fig. 2** BNWF model and implementation of the springs and dashpots

Fig. 3 Normalized load-normalized displacement curves of the nonlinear springs

Table 3 Foundations' dimensions considered for SMRFs

SMRF	Soil	Width (m)	Length (m)	Height (m)
3-story	B	1	26	0.6
	C	1	26	0.6
	D	1.1	27	0.7
	E	1.1	27	0.7
5-story	B	1.3	26	0.7
	C	1.3	26	0.7
	D	1.3	27	0.7
	E	1.3	27	0.7
7-story	B	1.5	27	0.8
	C	1.5	27	0.8
	D	2	27	0.8
	E	2	27	0.8
9-story	B	2.5	27	1.0
	C	2.5	27	1.0
	D	3	27	1.1
	E	3	27	1.1

assumed provisions and load combinations. Table 3 presents the dimensions of the foundation considered for SMRFs.

To define the materials used in the BNWF model, the equations presented by Boulanger et al. (Boulanger et al. 1999) were used. According to the definition, in the elastic region of *the QzSimple* material model, load q_e was assumed to have linear behavior regarding deformation, z.

$$q_e = k_{ini}z \tag{1}$$

where k_{ini} is the initial elastic stiffness. It is experimentally achieved that the elastic maximum load, q_0, is a factor C_r of the ultimate load, q_{ult}, then:

$$q_0 = C_r q_{ult} \tag{2}$$

Then, the nonlinear part of the curve can be defined by:

$$q = q_{ult} - (q_{ult} - q_0)\left[\frac{Cz_{50}}{Cz_{50} + |z - z_0|}\right]^n \tag{3}$$

where z_{50} is the displacement in the half of ultimate load, z_0 is displacement in the yield point, C and n are constitutive values to control the post-yield portion and curve shape. The calculation for *PxSimple* and *TxSimple* material models is similar to the *QzSimple* material model with assuming various values of C_r, n, C. Gazetas (Gazetas 1991) proposed the following equations for calculating the vertical stiffness and lateral stiffness of springs, k_v, and k_h, respectively, based on the width and length of foundation, B and L, respectively.

$$k_{\mathrm{v}} = \frac{GL}{1-\upsilon}\left[0.73 + 1.54\left(\frac{B}{L}\right)^{0.75}\right]$$

$$k_{\mathrm{h}} = \frac{GL}{2-\upsilon}\left[2 + 2.5\left(\frac{B}{L}\right)^{0.85}\right]$$

(4)

2.3 Numerical modeling approach to represent infill masonry wall

For decades, researchers experimentally studied the IMWs effects on the lateral response of RC and SMRFs (see (Buonopane and White 1999; Tasnimi and Mohebkhah 2011)), and proposed different types of numerical models (see Koutromanos et al. 2011, Trapani et al. 2018, Mazza 2019). For instance, the less complicated and simple model is a double strut element developed by Smyrou et al. (Smyrou et al. 2011), three nonparallel strut elements that consider the interaction between IMWs and frames were developed by El-Dakhakhni et al. (El-Dakhakhni et al. 2003). Crisafulli and Carr (Crisafulli and Carr 2007) developed four nodes panel connected to the beam and column joints to include both shear and compressive behavior of IMW. In this research, the model proposed by Rodrigues et al. (2010) that is commonly used for simulation of nonlinear behavior of IMWs was used. Figure 4 presents the schematic illustration of the IMW modeling approach in Opensees (McKenna et al. 2016). Some experimental tests assuming cyclic loads validated this model. Therefore, to validate the modeling process, the experimental test used by Kakaletsis and Karayannis (Kakaletsis and Karayannis 2008) was assumed. Figure 5 presents the shear-displacement curve of the IMW model validated with the result of Test S-full infill used by Kakaletsis and Karayannis (Kakaletsis and Karayannis 2008). The results show good agreement with the numerical modeling of IMW.
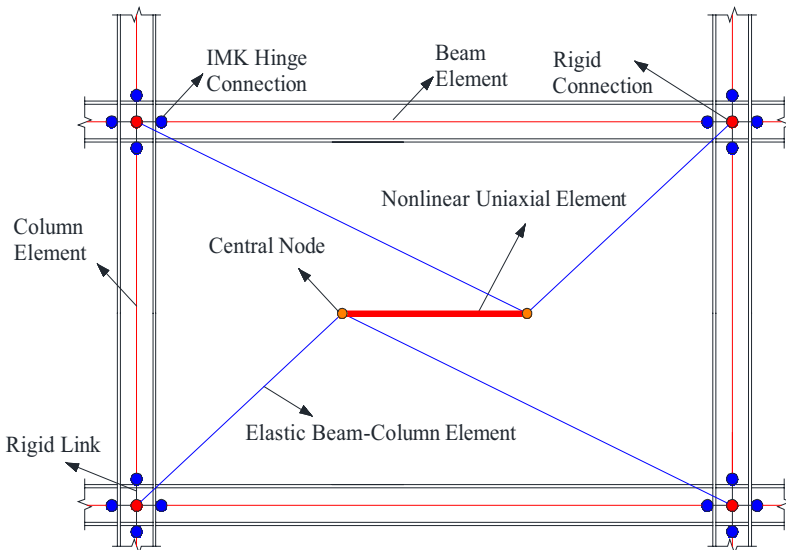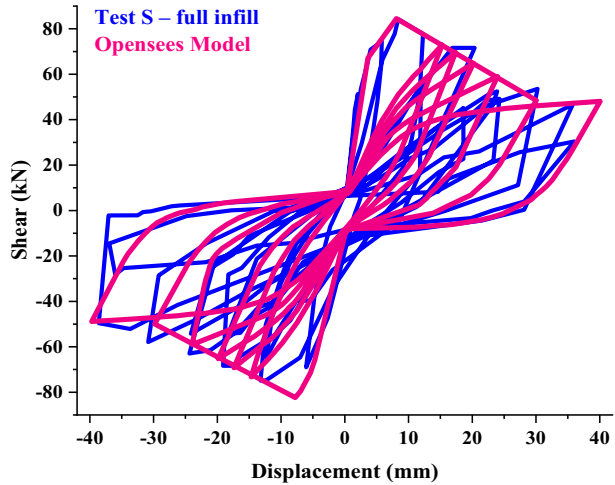

Fig. 4 Schematic illustration of IMW modeling approach in Opensees (McKenna et al. 2016)

Fig. 5 Verification of shear-displacement curve of IMW model in Opensees with the result of Test S-full infill used by Kakaletsis and Karayannis (Kakaletsis and Karayannis 2008)

To define the IMW model, the nonlinear uniaxial element (see Fig. 4) should characterize by a multi-linear hysteresis curve defined as *uniaxial Material Pinching4* in Opensees (McKenna et al. 2016). Furtado et al. (Furtado et al. 2015, 2016b, 2018, 2021) numerically investigated the IMWs and their influences on the seismic structural behavior. They showed that the first cracks of IMW could appear between 0.075% and 0.12% drift (d_c). Therefore, in this study, d_c was selected equal to 0.1%, and the corresponding cracking force, F_c, was determined equal to 570 kPa, based on the relationship between elasticity modulus of IMW, E_m, and d_c. According to experimental tests and recommendations of seismic codes, the ratio of cracking strength and maximum strength (F_c/F_{cr}) for the IMW considering the brick and mortar properties can be adopted equal to 0.55 (Furtado et al. 2015). In addition, F_y and d_y are the yielding force and the corresponding displacement that can be assumed between 65 and 75% of F_{cr} and 0.35–0.50% of d_c, while F_{cr} can occur for drift value of 0.5% (Furtado et al. 2021). Moreover, by estimating the diagonal compressive strength of IMW from experimental specimens, f_{IMW}, the maximum strength can be calculated from the following equations:

$$F_{cr} = 0.818 \frac{L_{inf} \times t_{inf} \times f_{IMW}}{C_t}(1 + \sqrt{C_t^2 + 1})$$

$$C_t = 1.925 \frac{L_{inf}}{h_{inf}}$$

(5)

where L_{inf}, h_{inf}, t_{inf} are the length, height, and thickness of the assumed IMW. Table 4 illustrates modeling properties used for IMWs. Figure 6 presents the uniaxial material model adopted for numerical modeling of IMW according to Table 4.

Table 4 Numerical properties adopted for modeling IMWs (Furtado et al. 2021)

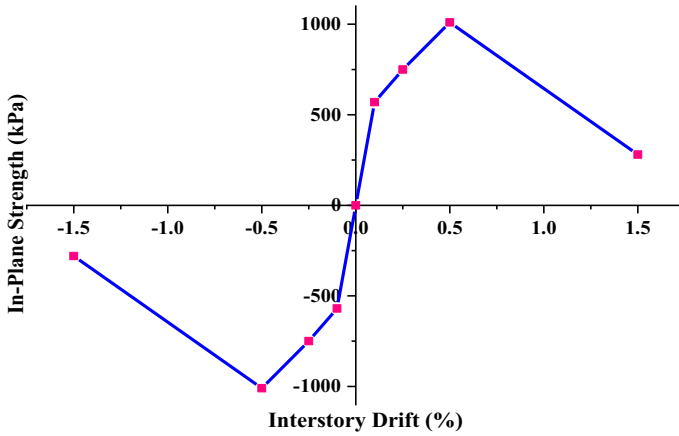| d_c(%)	d_y(%)	d_{cr}(%)	d_u(%)	F_c(kPa)	F_y(kPa)	F_{cr}(kPa)	F_u(kPa)
0.1	0.25	0.5	1.5	570	750	1010	280

Fig. 6 The uniaxial material model was adopted for numerical modeling of IMW according to Table 4
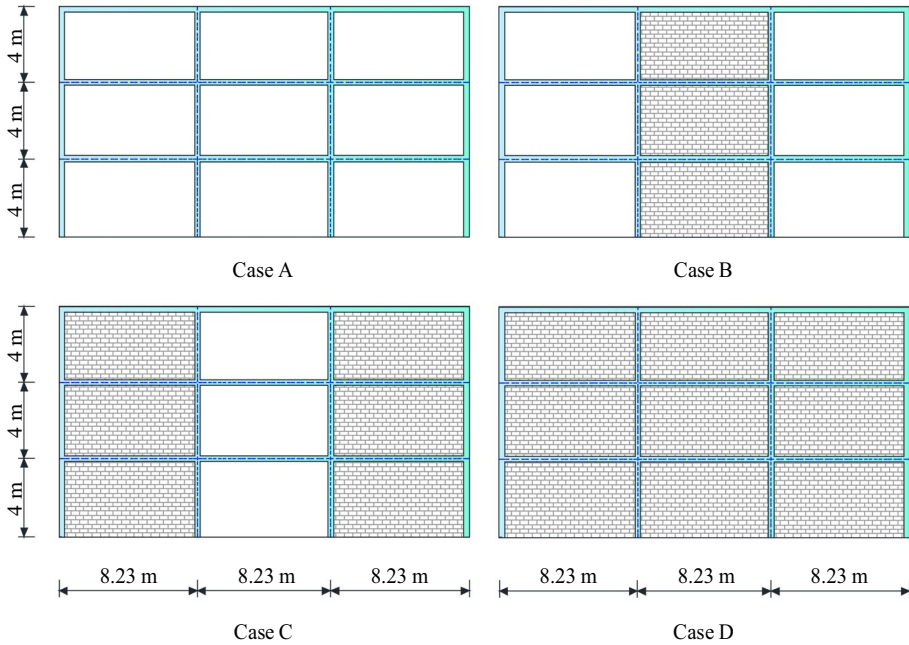

Fig. 7 Illustration of different placement of IMWs considered for the 3-Story SMRF model

2.4 Numerical models

To investigate the effects of assuming IMWs and SSI in the 3-Story, 5-Story, 7-Story, and 9-Story SMRFs, four placements of IMWs were considered. Figure 7 presents different placement of IMWs considered for the 3-Story SMRF. Similarly, all these placements were considered for other SMRFs with and without SSI effects.

Table 5 Fundamental periods of SMRFs with and without IMWs

SMRF	Soil type	Case A	Case B	Case C	Case D
3-story	B	1.17	1.09	1.0	0.95
	C	1.01	0.96	0.90	0.87
	D	1.0	0.96	0.90	0.87
	E	1.0	0.95	0.89	0.86
5-story	B	1.81	1.69	1.57	1.50
	C	1.66	1.57	1.48	1.42
	D	1.56	1.49	1.41	1.36
	E	1.56	1.49	1.41	1.36
7-story	B	2.44	2.28	2.12	2.02
	C	2.14	2.04	1.93	1.86
	D	2.12	2.02	1.91	1.85
	E	2.11	2.01	1.90	1.83
9-story	B	2.75	2.60	2.44	2.34
	C	2.55	2.43	2.31	2.23
	D	2.42	2.32	2.21	2.15
	E	2.40	2.35	2.24	2.17

Table 5 presents fundamental periods of SMRFs with and without IMWs assuming different cases and soil types. In each soil type, Case D had the lowest fundamental period and Case A had the highest one. It is worth noting that the vibration mode of structures were influenced by adding IMWs. For instance, in Case B, the values of the first vibration mode was increased by 2.33%, as compared to Case A. Moreover, in Case C and D, the values of the first vibration mode were increased by 4.67 and 6.07%, respectively. Regarding different placement of IMWs, structure founded on soil type E had the lowest fundamental period and structure founded on soil type B had the highest one. Therefore, the fundamental period of structures were affected by changing the soil types.

3 Incremental dynamic analysis

It is important to evaluate the current state of a building after a severe earthquake. The state of a building can be defined based on damage states of the non-structural and structural members. Seismic codes propose useful tools to determine the seismic performance levels of the structures. To investigate the seismic performance levels of SMRFs, IDA was employed to determine the seismic limit-states of SMRFs regarding the increasing amount of Intensity Measure (IM). In this study, the spectral acceleration in the fundamental period of the SMRF, $S_a(T_1)$, was selected as IM, and the Maximum Interstory Drift Ratio (M-IDR) as controlling parameter. Then, the seismic limit-state capacity assessment of SMRFs was conducted by performing IDAs assuming the Far-Fault (FF) records introduced by FEMA-P695 (FEMA P695 2009). In addition, FEMA 356 (FEMA-356. 2000) propose three performance levels of Immediate Occupancy (IO), Life Safety (LS), and Collapse Prevention (CP) for corresponding M-IDR of 0.7%, 2.5%, and 5.0%, respectively, which can be used for limit-state assessment. Moreover, the Total Collapse (TC) limit of the structure can be achieved by considering the flat part of the IDA curve.
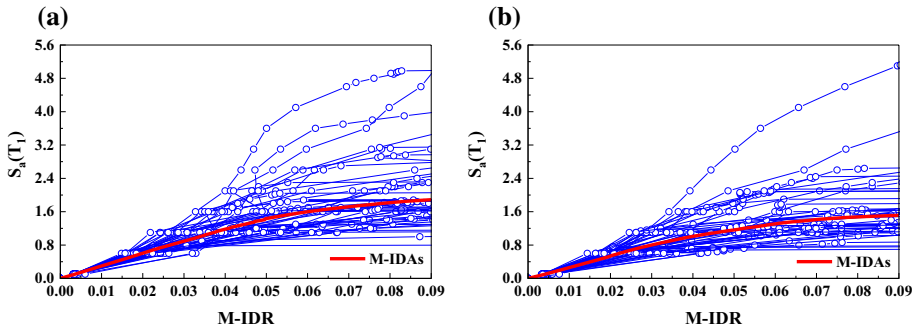
Fig. 8 IDA curves of the 3-story SMRF, **a** without SSI, and, **b** with SSI, in the soil D subjected to FF record subset
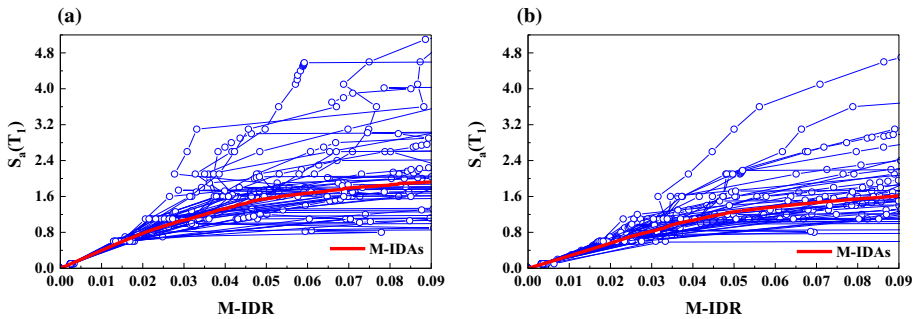

Fig. 9 IDA curves of the 3-story SMRF, **a** with IMWs (Case D), and, **b** without IMWs (Case A), in the soil C subjected to FF record subset

According to a full-scale experimental test of RC structure done by Pujol and Fick (Pujol and Fick 2010), IMWs that were assumed to fill all bays from bottom to top witnessed initial cracks with the width of 4 mm in M-IDR of 0.25%. Their results confirmed that IMWs were in the collapse state at an M-IDR of 1.75%. Therefore, in this M-IDR, IMWs were collapsed and could not be considered in the numerical model. To assume the collapse effects of IMWs, a Tcl programming algorithm was developed in OpenSees (McKenna et al. 2016) to control the collapse of IMWs in each story assuming M-IDR of the collapse limit of IMWs equal to 1.75%. Figure 8 presents IDAs of the 3-story SMRF neglecting and including SSI effects in the soil D subjected to FF record subset. Figure 9 presents IDAs of the 3-story SMRF with IMWs (Case D) and without IMWs (Case A) in soil C subjected to FF record subset.

3.1 Seismic performance level

To evaluate the influence of considering IMWs in modeling, the seismic performance levels of each aforementioned case based on the median IDA curves (M-IDAs) were compared. Figure 10a–d present M-IDA curves of the 3-Story SMRF considering four cases of IMWs placement and four soil types of B, C, D, and E, respectively, subjected to FF record subset. According to Fig. 10a–b, Case D had higher values of M-IDAs and showed
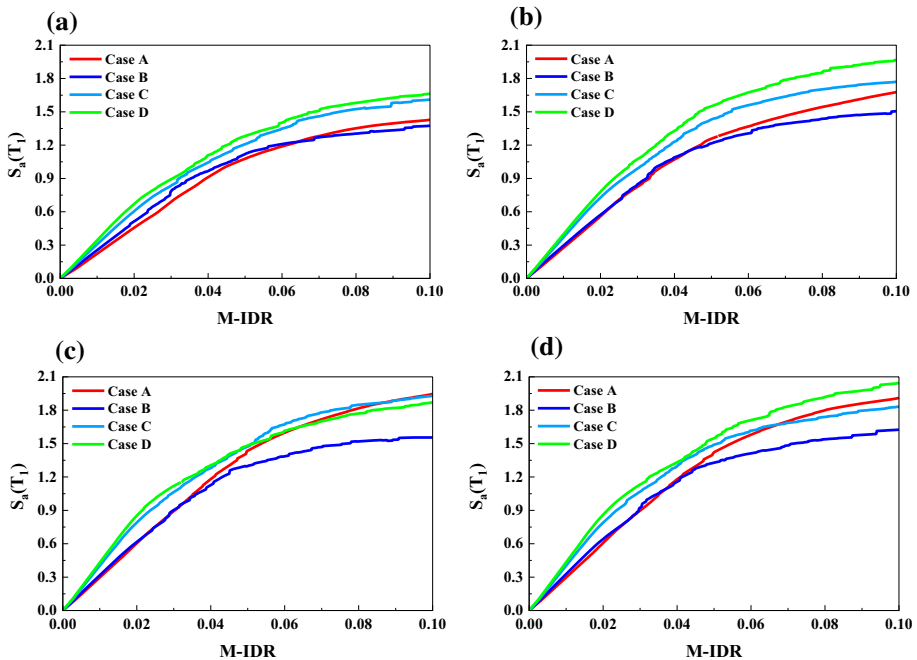
Fig. 10 M-IDAs of the 3-Story SMRF considering four cases of IMWs, **a** soil B, **b** soil C, **c** soil D, and **d** soil E, subjected to FF record subset

that the placement of IMWs in all floor levels increased the lateral resisting strength of the 3-Story SMRF. While, the placement of IMWs according to Case C had lower values of M-IDAs compared to Case D, and higher values than other cases. Therefore, increasing the placement of IMWs in the 3-Story SMRF with soil types of B and C showed an increase in the values of $S_a(T_1)$ in M-IDA curves. For cases in the soil types of D and E presented in Fig. 10c, d, respectively, the placement of IMWs in the 3-Story SMRF increased the values of $S_a(T_1)$ in M-IDA curves. In all soil types, the placement of IMWs according to Case B had lower values of $S_a(T_1)$ in M-IDA curves that show the negative effects of using this case for the 3-Story SMRF. It can be concluded that having an opening in the 3-Story SMRF (i.e. Case B) can significantly decrease the values of $S_a(T_1)$. Similar results were obtained from M-IDA curves of the 3-Story SMRF considering four cases of IMWs with SSI effect presented in Fig. 11a–d.

To compare between results of all cases and soil types, the seismic limit-state capacities of the 3-Story SMRF in four soil types according to the aforementioned seismic performance level are presented in Table 6. It is possible to compare the values of $S_a(T_1)$ in four performance levels of IO, LS, CP, and TC, and four soil types, assuming different placement of IMWs. For instance, assuming Case D in soil types of B, C, D, and E, the limit-state capacities of the 3-Story SMRF experienced an increase by 16.45% (from 1.428 to 1.663), 17.22% (from 1.428 to 1.663), − 3.9% (from 1.428 to 1.663), and 6.95% (from 1.428 to 1.663), respectively.

Table 7 presents the seismic limit-state capacities of the 3-Story SMRF in four soil types with SSI effects subjected to FF record subset. This table prepares the effects of
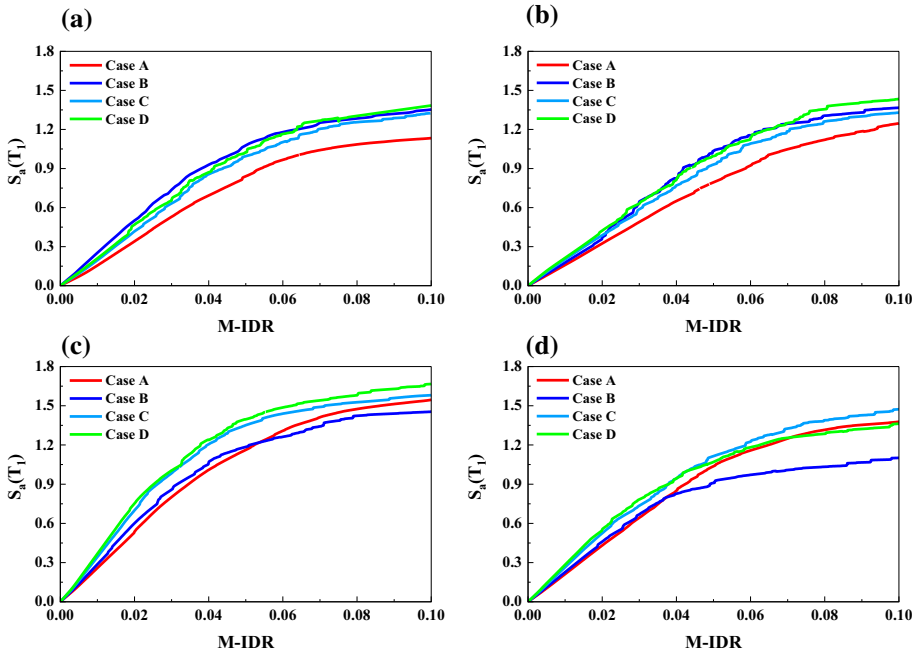
Fig. 11 M-IDAs of the 3-Story SMRF considering four cases of IMWs with SSI effect on the, **a** soil B, **b** soil C, **c** soil D, and **d** soil E, subjected to FF record subset

Table 6 Seismic limit-state capacities of the 3-Story SMRF in four cases assuming FF record subset

Performance level	IO	LS	CP	TC	IO	LS	CP	TC
3-Story SMRF	Soil B				Soil C			
Case A	0.152	0.564	1.077	1.428	0.191	0.708	1.258	1.678
Case B	0.177	0.645	1.118	1.374	0.209	0.700	1.216	1.505
Case C	0.213	0.735	1.208	1.610	0.257	0.869	1.431	1.770
Case D	0.238	0.792	1.281	1.663	0.277	0.936	1.550	1.967
3-Story SMRF	Soil D				Soil E			
Case A	0.206	0.754	1.436	1.948	0.206	0.761	1.422	1.911
Case B	0.222	0.752	1.298	1.555	0.228	0.766	1.328	1.625
Case C	0.277	0.931	1.473	1.930	0.277	0.932	1.490	1.832
Case D	0.297	1.006	1.482	1.872	0.299	1.015	1.547	2.044

SSI and can be easily used for comparing assumed cases. For example, in Case A with and without assuming SSI effects, the performance level of TC in soil B decreased from 1.428 (Table 6) to 1.133 (Table 7). Moreover, the values of $S_a(T_1)$ in four performance levels of IO, LS, CP, and TC, similarly decreased due to SSI effects. Therefore, the SSI effects can significantly affect the limit-state capacities.

Figure 12a–d present M-IDA curves of the 5-Story SMRF considering four cases of IMWs placement and four soil types of B, C, D, and E, respectively, subjected to

Table 7 Seismic limit-state capacities of the 3-Story SMRF with SSI effects assuming FF record subset

Performance level	IO	LS	CP	TC	IO	LS	CP	TC
3-Story SMRF	Soil B				Soil C			
Case A	0.102	0.438	0.840	1.133	0.111	0.406	0.794	1.247
Case B	0.174	0.631	1.077	1.352	0.124	0.502	1.035	1.366
Case C	0.133	0.520	0.994	1.326	0.144	0.483	0.930	1.329
Case D	0.145	0.570	1.023	1.384	0.154	0.518	0.995	1.435
3-Story SMRF	Soil D				Soil E			
Case A	0.177	0.679	1.162	1.545	0.146	0.534	1.037	1.378
Case B	0.197	0.724	1.185	1.454	0.158	0.553	0.909	1.101
Case C	0.233	0.873	1.351	1.581	0.183	0.645	1.114	1.473
Case D	0.250	0.895	1.396	1.666	0.198	0.673	1.069	1.362
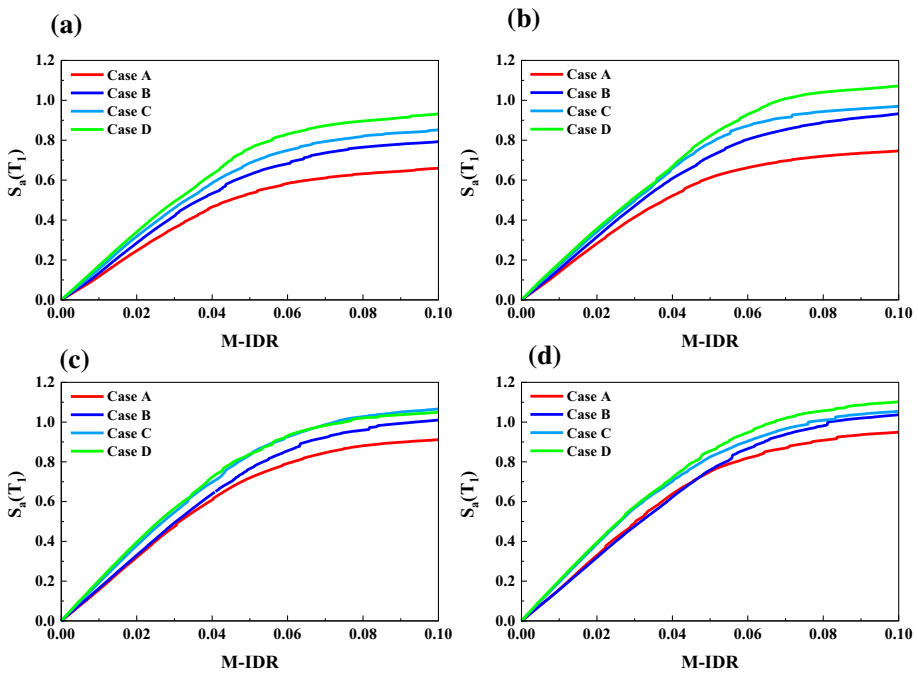
Fig. 12 M-IDAs of the 5-Story SMRF considering four cases of IMWs, **a** soil B, **b** soil C, **c** soil D, and **d** soil E, subjected to FF record subset

FF record subset. According to Fig. 12a, b, Case D had higher values of M-IDAs and showed that the placement of IMWs in all floor levels significantly increased the lateral resisting strength of the 5-Story SMRF. In addition, the placement of IMWs according to Case C had lower values of M-IDAs compared to Case D, and higher values than other cases. It can be noted that increasing the IMWs can significantly affect the $S_a(T_1)$ values of M-IDA of the 5-Story SMRF with soil types of B and C. Similar results were observed for soil D and soil E in Fig. 12c, d, respectively. Moreover, it can be show that
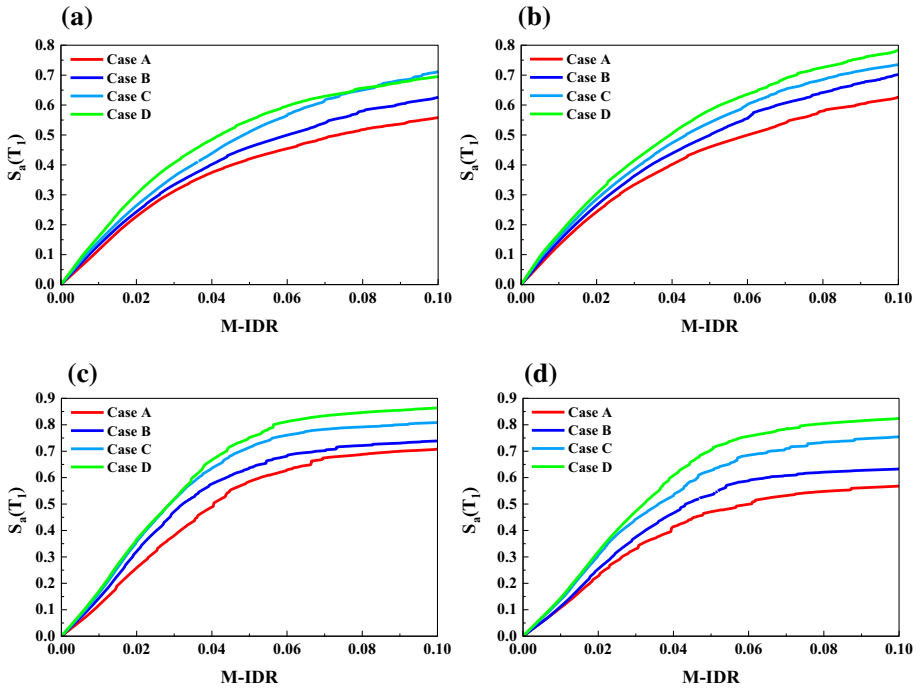
Fig. 13 M-IDAs of the 5-Story SMRF considering four cases of IMWs with SSI effect on the, **a** soil B, **b** soil C, **c** soil D, and **d** soil E, subjected to FF record subset

the effects of the placement of IMWs in the 5-Story SMRF in soil types of B and C is more than those in soil types of D and E. The main reason for this may be lie in the type of structural elements. The 5-Story SMRF had higher structural strength in soil type E comparing with soil type B and for this reason, fundamental period of the 5-Story SMRF in soil E is less than in soil B (e.g. 1.56 and 1.81, respectively, according to Case

Table 8 Seismic limit-state capacities of the 5-Story SMRF in four cases assuming FF record subset

Performance level	IO	LS	CP	TC	IO	LS	CP	TC
3-Story SMRF	Soil B				Soil C			
Case A	0.090	0.305	0.532	0.659	0.094	0.351	0.612	0.746
Case B	0.090	0.356	0.628	0.792	0.104	0.395	0.718	0.933
Case C	0.106	0.389	0.686	0.852	0.122	0.422	0.786	0.970
Case D	0.119	0.420	0.759	0.932	0.131	0.435	0.821	1.071
3-Story SMRF	Soil D				Soil E			
Case A	0.109	0.401	0.719	0.912	0.109	0.417	0.751	0.949
Case B	0.114	0.412	0.765	1.010	0.109	0.399	0.758	1.037
Case C	0.135	0.467	0.834	1.066	0.137	0.478	0.824	1.054
Case D	0.143	0.485	0.839	1.049	0.143	0.486	0.854	1.101

A in Table 5). Therefore, the structural elements are important factor in the collapse of structure and can increase the values of $S_a(T_1)$ in M-IDA curves.

Figure 13a–d present M-IDA curves of the 5-Story SMRF considering four cases of IMWs and four soil types with SSI effect subjected to FF record subset. The SSI effects can significantly reduce the values of $S_a(T_1)$ in M-IDA curves of all cases. Therefore, it is suggested to consider the SSI effects in the evaluation process due to its high influence.

Table 8 presents seismic limit-state capacities of the 5-Story SMRF in four cases of IMWs and four soil types assuming FF record subset. It can be seen that the placement of IMWs in all cases can significantly affect the values of $S_a(T_1)$ in M-IDA curves in all seismic limit-state capacities. For instance, in soil type B, assuming IMWs placement of Case B, Case C, and Case D increased the performance level of TC of the 5-Story SMRF by 41.42%, 29.28%, and 20.18%, respectively. In addition, for soil type C, the performance level of TC of the 5-Story SMRF increased by 43.56%, 30.02%, and 25.06%, respectively. Table 9 presents seismic limit-state capacities of the 5-Story SMRF with SSI effects subjected to FF record subset. The SSI effects can significantly reduce the $S_a(T_1)$ values in M-IDA curves. For instance, in soil type E, the $S_a(T_1)$ values in the performance level of CP for Cases of A to D decreased by 37.41% (from 0.751 to 0.470), 29.55% (from 0.758 to 0.534), 24.27% (from 0.828 to 0.627), and 17.44% (from 0.854 to 0.705), respectively. Therefore, it is suggested to the designers for assuming the effects of IMWs and SSI in their evaluations, and Tables 8 and 9 can be easily used for the prediction of IMWs and SSI effects.

Figure 14a–d present M-IDA curves of the 7-Story SMRF considering four cases of IMWs placement and four soil types of B, C, D, and E, respectively, subjected to FF record subset. Results presented by Fig 14a and b showed that Case D had higher values of M-IDAs compared to other cases. While Case B decreased the values of M-IDAs of the 7-Story SMRF founded on soil type B, other cases had a positive influence on the values of M-IDAs of the 7-Story SMRF. Therefore, the placement of IMWs can significantly increase the values of $S_a(T_1)$ in M-IDA curves of the 7-Story SMRF founded on soil types of B and C. Figure 14c and d show that the placement of IMWs can affect the values of $S_a(T_1)$ in M-IDA curves in a positive way, while the number of values between cases has small differences. It should be noted that the 7-Story SMRF founded on soil types of D and E had higher structural strength compared to corresponding to the 7-Story SMRF founded

Table 9 Seismic limit-state capacities of the 5-Story SMRF with SSI effects assuming FF record subset

| Performance level	IO	LS	CP	TC	IO	LS	CP	TC
3-Story SMRF	Soil B				Soil C			
Case A	0.070	0.273	0.420	0.557	0.093	0.025	0.459	0.626
Case B	0.104	0.315	0.499	0.702	0.104	0.315	0.499	0.702
Case C	0.103	0.314	0.510	0.711	0.117	0.338	0.541	0.735
Case D	0.116	0.359	0.549	0.696	0.125	0.364	0.583	0.783
3-Story SMRF	Soil D				Soil E			
Case A	0.079	0.319	0.585	0.707	0.074	0.285	0.470	0.567
Case B	0.098	0.396	0.637	0.739	0.075	0.318	0.534	0.632
Case C	0.110	0.440	0.714	0.808	0.094	0.384	0.627	0.754
Case D	0.116	0.444	0.751	0.863	0.099	0.401	0.705	0.823
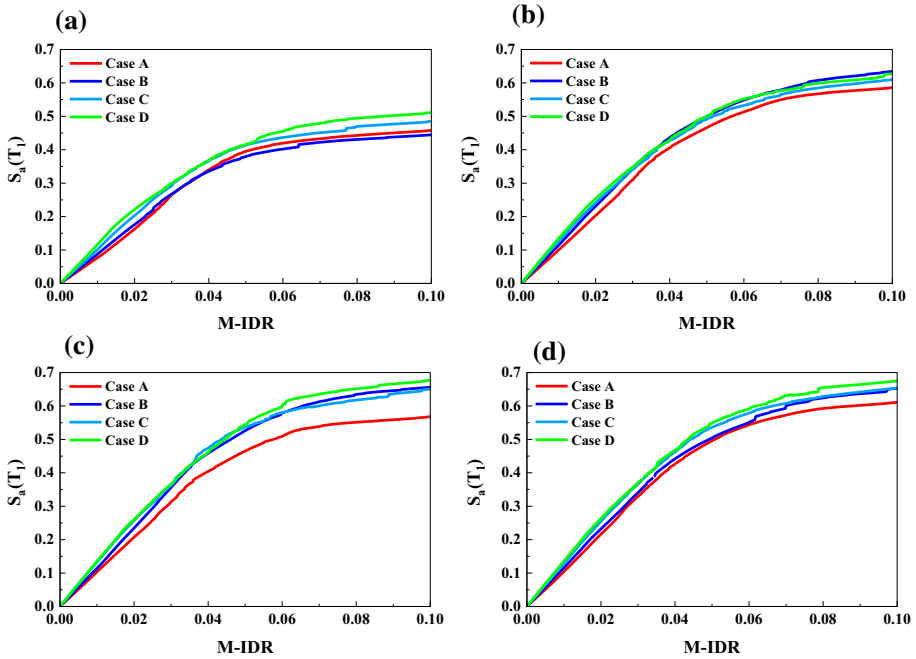
Fig. 14 M-IDAs of the 7-Story SMRF considering four cases of IMWs, **a** soil B, **b** soil C, **c** soil D, and **d** soil E, subjected to FF record subset
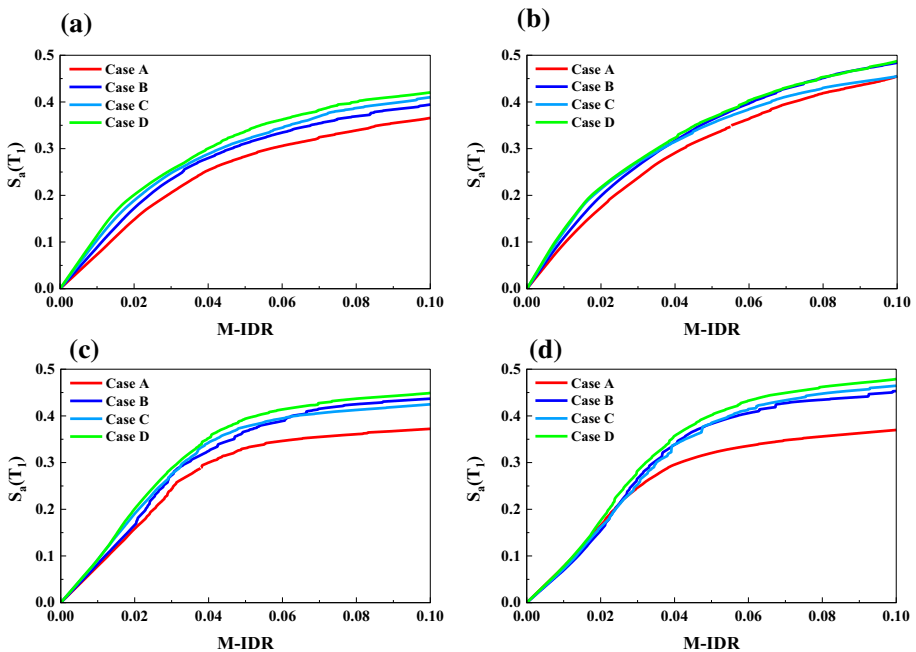
Fig. 15 M-IDAs of the 7-Story SMRF considering four cases of IMWs with SSI effect on the, **a** soil B, **b** soil C, **c** soil D, and **d** soil E, subjected to FF record subset

Table 10 Seismic limit-state capacities of the 7-Story SMRF in four cases assuming FF record subset

Performance level	IO	LS	CP	TC	IO	LS	CP	TC
3-Story SMRF	Soil B				Soil C			
Case A	0.053	0.209	0.395	0.458	0.069	0.253	0.466	0.586
Case B	0.061	0.219	0.380	0.444	0.079	0.286	0.499	0.634
Case C	0.070	0.251	0.413	0.484	0.088	0.290	0.492	0.609
Case D	0.081	0.261	0.415	0.511	0.094	0.303	0.501	0.627
3-Story SMRF	Soil D				Soil E			
Case A	0.072	0.257	0.464	0.568	0.071	0.272	0.495	0.611
Case B	0.080	0.294	0.525	0.656	0.081	0.285	0.504	0.652
Case C	0.093	0.309	0.536	0.650	0.090	0.312	0.536	0.654
Case D	0.095	0.315	0.544	0.677	0.095	0.318	0.549	0.674

on soil types of B and C (see Table 2). It can be concluded that the placement of IMWs effects can increase the structural strength of the SMRF. Figure 15a–d present M-IDA curves of the 7-Story SMRF considering four cases of IMWs and four soil types with SSI effect subjected to FF record subset. Although the SSI effect decreased the $S_a(T_1)$ values of bare frames in all soil types (e.g. Case A), assuming SSI significantly affects M-IDA curves of the SMRFs with IMWs (e.g. Case B, Case C, and Case D). In other words, the $S_a(T_1)$ values of M-IDAs for the 7-Story SMRF considering SSI effects were lower than those for the 7-Story SMRF neglecting SSI effects. Therefore, SSI effects play a key role in seismic capacity evaluations and should be taken into account.

Table 10 presents seismic limit-state capacities of the 7-Story SMRF in four cases of IMWs and four soil types assuming FF record subset. Results showed that the placement of IMWs in all the cases increased the values of $S_a(T_1)$ in M-IDA curves of the 7-Story SMRF founded on soil type B. For instance, assuming IMWs placement of Case C and Case D, the performance level of TC of the 7-Story SMRF founded on soil type B increased by 5.67% and 11.57%, respectively. Table 11 presents seismic limit-state capacities of the 7-Story SMRF with SSI effects subjected to FF record subset. Compared to Table 10, SSI effects significantly decrease the values of $S_a(T_1)$ in M-IDA curves. In IMWs placement of Case B, Case C, and Case D, the performance level of TC

Table 11 Seismic limit-state capacities of the 7-Story SMRF with SSI effects assuming FF record subset

| Performance level	IO	LS	CP	TC	IO	LS	CP	TC
3-Story SMRF	Soil B				Soil C			
Case A	0.051	0.179	0.283	0.365	0.068	0.207	0.329	0.455
Case B	0.062	0.206	0.311	0.394	0.078	0.233	0.362	0.484
Case C	0.073	0.220	0.319	0.410	0.087	0.243	0.354	0.455
Case D	0.080	0.229	0.337	0.420	0.093	0.247	0.366	0.487
3-Story SMRF	Soil D				Soil E			
Case A	0.054	0.198	0.330	0.372	0.053	0.210	0.320	0.369
Case B	0.057	0.224	0.367	0.436	0.048	0.211	0.383	0.453
Case C	0.063	0.234	0.376	0.424	0.050	0.209	0.385	0.464
Case D	0.064	0.246	0.394	0.449	0.053	0.233	0.401	0.478
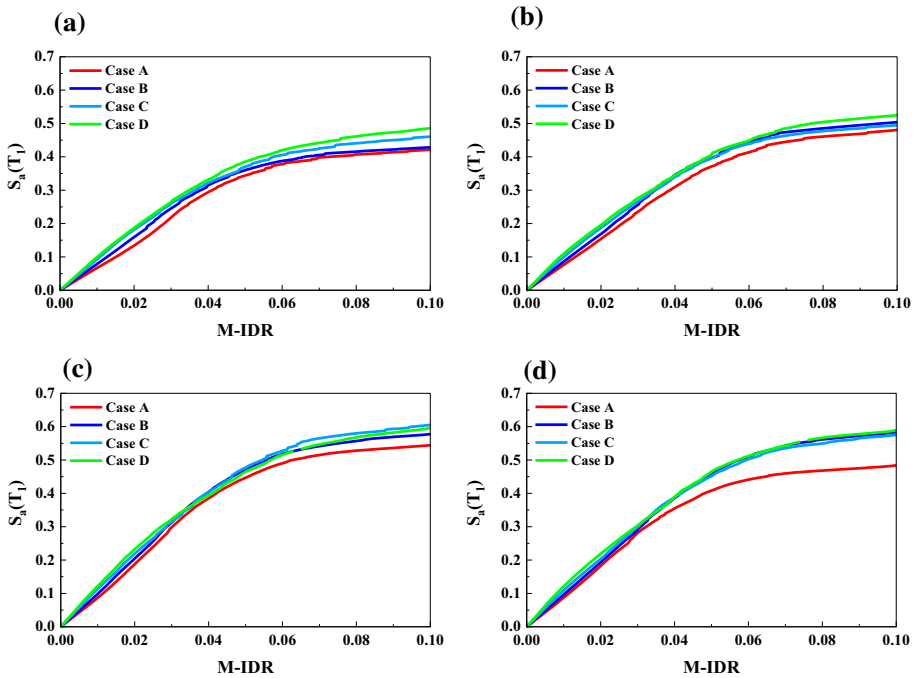
Fig. 16 M-IDAs of the 9-Story SMRF considering four cases of IMWs, **a** soil B, **b** soil C, **c** soil D, and **d** soil E, subjected to FF record subset

of the 7-Story SMRF founded on soil type B decreased by 7.94%, 12.32%, and 15.06%, respectively, assuming SSI effects. Similar trends were observed for other soil types.

Figure 16a–d present M-IDA curves of the 9-Story SMRF considering four cases of IMWs placement and four soil types of B, C, D, and E, respectively, subjected to FF record subset. Case D had higher values of M-IDAs compared to other cases in the four soil types, and Case A had the lowest values among other cases. Similar to other SMRFs, it can be seen that the placement of IMWs can significantly increase the values of $S_a(T_1)$ in M-IDA curves of the 9-Story SMRF. Figure 17a–d present M-IDA curves of the 9-Story SMRF considering four cases of IMWs and four soil types with SSI effect subjected to FF record subset. Compared to Fig. 16a–d, differences between Case D and Case A increased. In other words, the SSI effects had a lower influence on the cases with IMWs placement than the bare frame (e.g. Case A).

Tables 12 and 13 present seismic limit-state capacities of the 7-Story SMRF in four cases of IMWs and four soil types assuming FF record subset without and with SSI effects, respectively. Results confirm the increasing trends of the values of $S_a(T_1)$ in M-IDA curves of the 9-Story SMRF with the IMWs placement of Case B, Case C, and Case D. For instance, assuming IMWs placement of Case D, the performance level of TC of the 9-Story SMRF founded on soil type B increased by 15.2%, and with assuming the SSI effects, the performance level of TC increased by 15.48%. Results of tables can be used for estimating the effects of IMWs and SSI on the performance levels of the 9-Story SMRF.
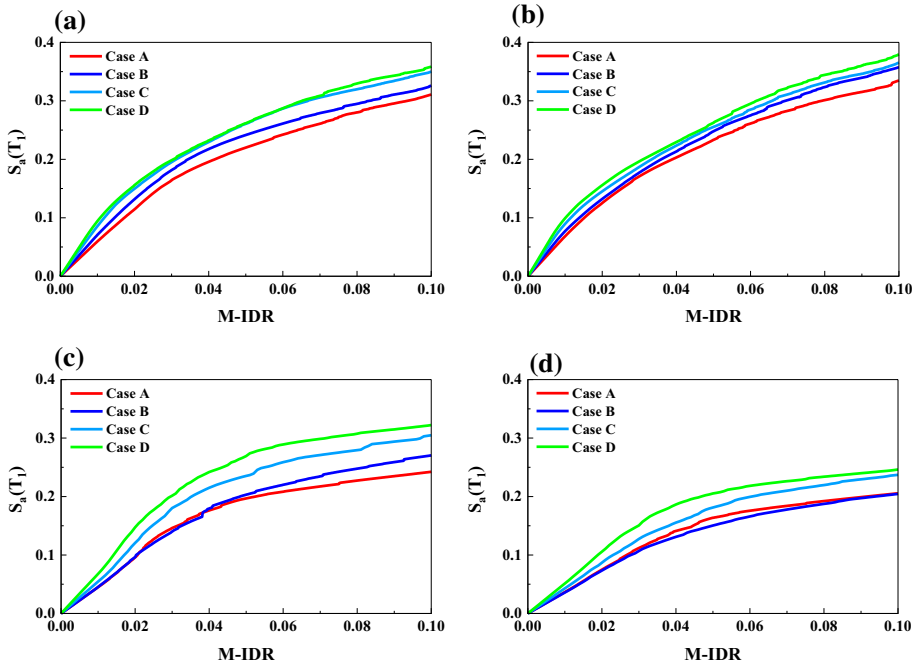
Fig. 17 M-IDAs of the 9-Story SMRF considering four cases of IMWs with SSI effect on the, **a** soil B, **b** soil C, **c** soil D, and **d** soil E, subjected to FF record subset

Table 12 Seismic limit-state capacities of the 9-Story SMRF in four cases assuming FF record subset

Performance level	IO	LS	CP	TC	IO	LS	CP	TC
3-Story SMRF	Soil B				Soil C			
Case A	0.047	0.172	0.334	0.421	0.053	0.194	0.371	0.481
Case B	0.055	0.202	0.360	0.428	0.060	0.213	0.397	0.503
Case C	0.065	0.218	0.370	0.460	0.071	0.227	0.396	0.494
Case D	0.070	0.226	0.385	0.485	0.079	0.238	0.407	0.524
3-Story SMRF	Soil D				Soil E			
Case A	0.060	0.239	0.446	0.544	0.060	0.229	0.408	0.484
Case B	0.068	0.256	0.473	0.577	0.067	0.242	0.458	0.583
Case C	0.080	0.265	0.477	0.605	0.077	0.253	0.451	0.575
Case D	0.087	0.281	0.464	0.595	0.087	0.262	0.465	0.589

4 Seismic fragility curves

In this section, the fragility curves of the aforementioned SMRFs were compared based on the analytical procedures and probability of reaching or exceeding the aforementioned damages states. It is important to evaluate the influence of IMWs placement and their effects on the seismic performance. Therefore, the performance levels of IO and LS, which present nonstructural damages without death or serious structural failure, were considered.

Table 13 Seismic limit-state capacities of the 9-Story SMRF with SSI effects assuming FF record subset

Performance level	IO	LS	CP	TC	IO	LS	CP	TC
3-Story SMRF	Soil B				Soil C			
Case A	0.041	0.141	0.220	0.310	0.048	0.148	0.233	0.334
Case B	0.049	0.157	0.241	0.326	0.055	0.155	0.247	0.357
Case C	0.060	0.173	0.260	0.350	0.065	0.166	0.255	0.365
Case D	0.067	0.179	0.261	0.358	0.073	0.177	0.262	0.379
3-Story SMRF	Soil D				Soil E			
Case A	0.031	0.127	0.196	0.242	0.025	0.093	0.163	0.205
Case B	0.031	0.120	0.203	0.270	0.025	0.090	0.150	0.204
Case C	0.038	0.152	0.235	0.304	0.030	0.106	0.181	0.237
Case D	0.047	0.177	0.269	0.322	0.035	0.131	0.205	0.246
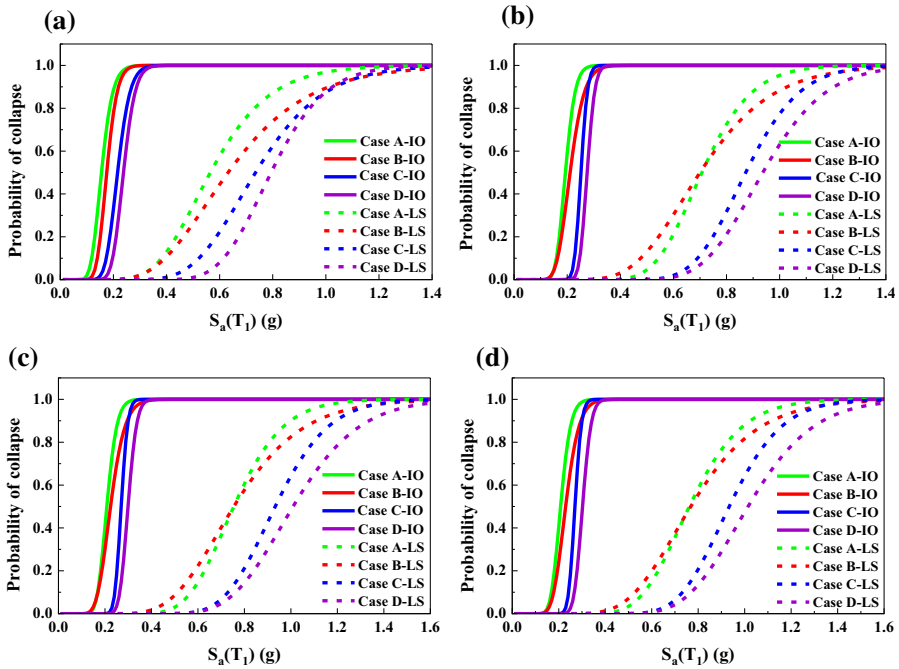
Fig. 18 Seismic fragility curves of the 3-Story SMRF considering four cases of IMWs on the, **a** soil type B, **b** soil type C, **c** soil type D, and **d** soil type E, subjected to FF record subset

According to the aforementioned performance levels, the probability of exceedance of a limit state (i.e. IO or LS) was determined and different cases were compared. It is worth noting that the difference between seismic fragility curves of IO and LS performance levels for the 9-story SMRF can be justified due to difference between their corresponding M-IDR.

Figure 18a–d illustrate seismic fragility curves in the performance of IO and LS of the 3-Story SMRF considering four cases of IMWs founded on the four soil types subjected

to FF record subset. The result shows that in the performance of IO for all soil types, the $S_a(T_1)$ values of Case D corresponding to the seismic failure probability of 50% are higher than those for Case C, Case B, Case A, respectively. According to Fig. 18a, in soil type B, the $S_a(T_1)$ values of Case A, Case B, Case C, and Case D, corresponding to the seismic collapse probability of 50% in the performance level of IO are 0.15, 0.17, 0.21, and 0.24, respectively, and in the performance level of LS are 0.56, 0.64, 0.74, and 0.79, respectively. Therefore, Case D with the full placement of IMWs can increase the seismic failure probability of the 3-Story SMRF founded on soil type B by 60% and 41.07%, in the performance of IO and LS, respectively. According to Fig. 18b, in soil type C, the $S_a(T_1)$ values of Case A, Case B, Case C, and Case D, corresponding to the seismic collapse probability of 50% in the performance level of IO are 0.19, 0.21, 0.25, and 0.27, respectively, and in the performance of LS are 0.70, 0.70, 0.87, and 0.94, respectively. Therefore, Case D with the full placement of IMWs can increase the seismic failure probability of the 3-Story SMRF founded on soil type C by 42.10% and 34.28%, in the performance of IO and LS, respectively. According to Fig. 18c, in soil type D, the $S_a(T_1)$ values of Case A, Case B, Case C, and Case D, corresponding to the seismic collapse probability of 50% in the performance level of IO are 0.21, 0.22, 0.28, and 0.30, respectively, and in the performance of LS are 0.75, 0.75, 0.93, and 1.01, respectively. Therefore, Case D with the full placement of IMWs can increase the seismic failure probability of the 3-Story SMRF founded on soil type D by 42.85% and 34.66%, in the performance of IO and LS, respectively. According to Fig. 18d, in soil type E, the $S_a(T_1)$ values of Case A, Case B, Case C, and Case D, corresponding to the seismic collapse probability of 50% in the performance level of IO are 0.21, 0.23, 0.28, and 0.30, respectively, and in the performance level of LS are 0.76, 0.77, 0.93, and 1.02, respectively. Therefore, Case D with the full placement of IMWs can increase the seismic
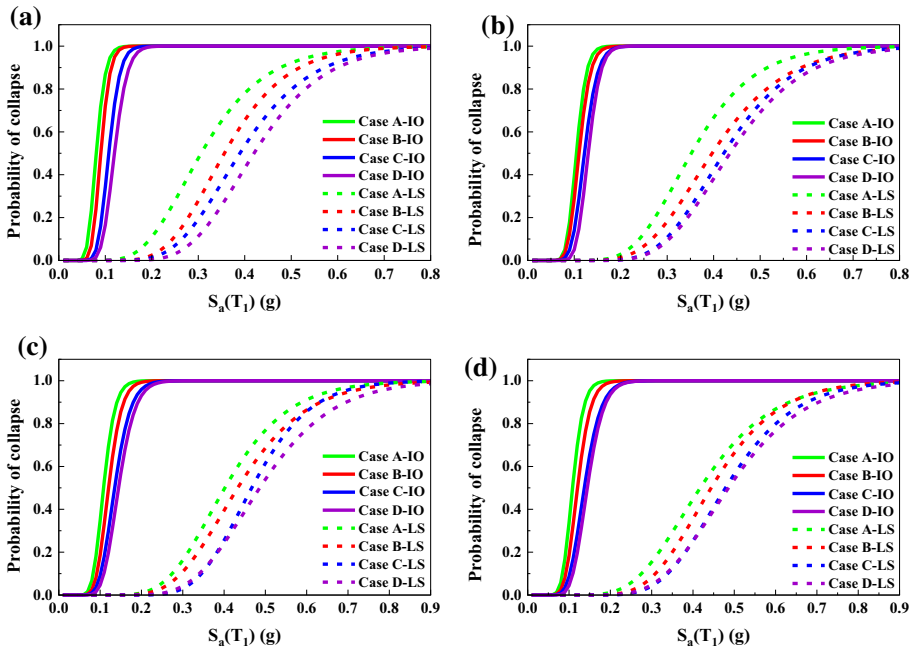

Fig. 19 Seismic fragility curves of the 5-Story SMRF considering four cases of IMWs on the, **a** soil type B, **b** soil type C, **c** soil type D, and **d** soil type E, subjected to FF record subset
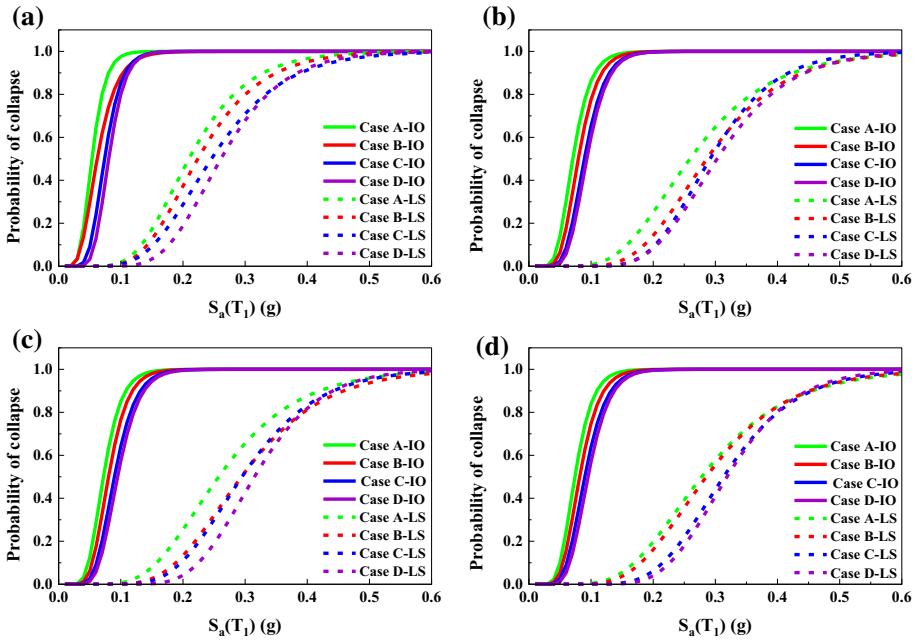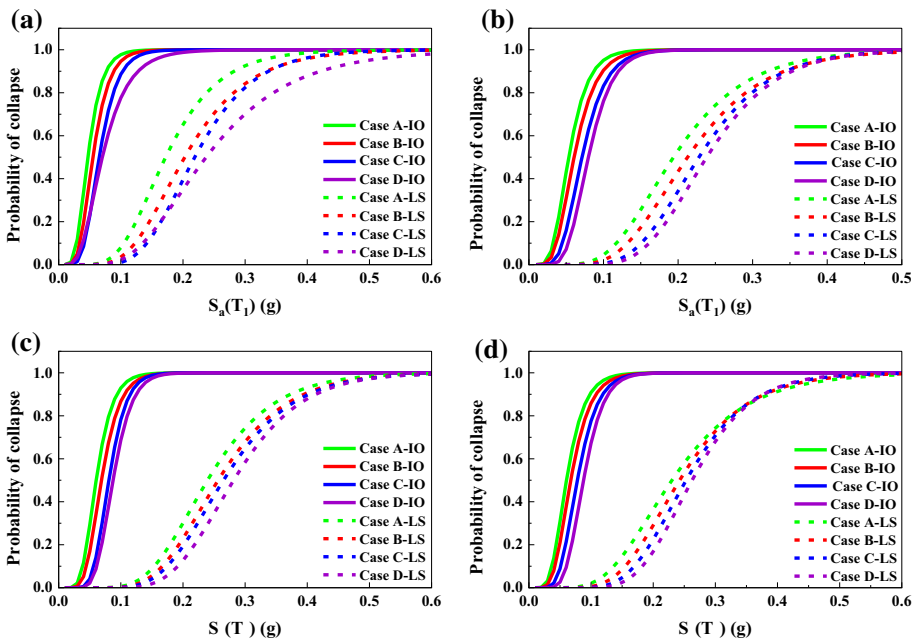
Fig. 20 Seismic fragility curves of the 7-Story SMRF considering four cases of IMWs on the, **a** soil type B, **b** soil type C, **c** soil type D, and **d** soil type E, subjected to FF record subset

Fig. 21 Seismic fragility curves of the 9-Story SMRF considering four cases of IMWs on the, **a** soil type B, **b** soil type C, **c** soil type D, and **d** soil type E, subjected to FF record subset

failure probability of the 3-Story SMRF founded on soil type E by 33.33% and 34.21%, in the performance of IO and LS, respectively.

Figures 19a–d, 20a–d, and 21a–d illustrate seismic fragility curves in the performance levels of IO and LS of the 5-Story, 7-Story, and 9-Story SMRFs considering four cases of IMWs founded on the four soil types subjected to FF record subset, respectively. According to Fig. 19a–d, comparing the Case A and Case D in the performance level of IO show that the seismic failure probability of the 5-Story SMRF founded on soil type B, C, D, and E increased by 48.75%, 39.36%, 31.19%, and 31.19%, respectively. Moreover, the performance level of LS experienced an increase by a factor of 37.70%, 23.93%, 20.94%, and 16.54%, respectively. According to Fig. 20a–d, comparing the Case A and Case D in the performance level of IO show that the seismic failure probability of the 7-Story SMRF founded on soil type B, C, D, and E increased by 52.83%, 36.23%, 31.94%, and 33.80%, respectively. Moreover, the performance level of LS experienced an increase by a factor of 24.88%, 19.76%, 22.56%, and 16.91%, respectively. According to Fig. 21a–d, comparing the Case A and Case D in the performance level of IO show that the seismic failure probability of the 9-Story SMRF founded on soil type B, C, D, and E increased by 48.93%, 49.05%, 45%, and 45%, respectively. Moreover, the performance level of LS experienced an increase by a factor of 31.39%, 22.68%, 17.57%, and 14.41%, respectively.

In all soil types and SMRFs, the $S_a(T_1)$ values in the seismic failure probability of 50% corresponding to the performance levels of IO and LS in Case D were higher than those for Case C, Case B, and Case A. Moreover, it can be seen that assuming Case D for SMRFs founded on soil type B (e.g. 5-Story SMRF) resulted in the highest increase in the $S_a(T_1)$ values of seismic failure probability of 50% (e.g. 48.75%), as compared to the SMRFs founded in soil type E (e.g. 31.19%).
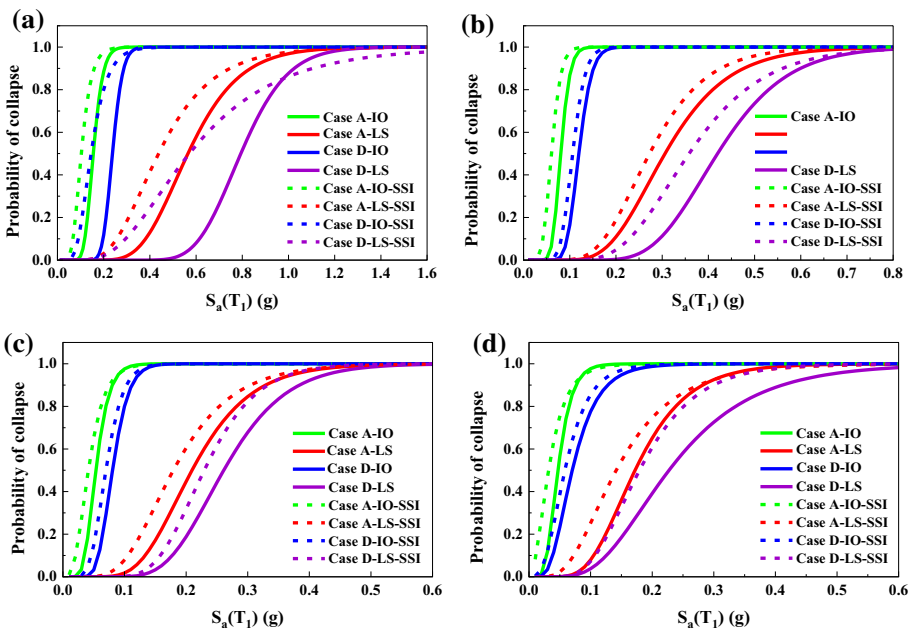

Fig. 22 Comparison of the seismic fragility curves of Case A and Case D on the soil type B with SSI effects, **a** the 3-Story, **b** the 5-Story, **c** the 7-Story, and **d** the 9-Story SMRFs, subjected to FF record subset

Therefore, it can be concluded that the IMWs can significantly decrease the seismic failure probability of the SMRFs and it should be assumed in the modeling process. The IMWs effects on the SMRFs founded on different soil types cannot be neglected and civil engineers should consider this effect to improve the seismic performance levels.

Figure 22a–d present the seismic fragility curves of the 3-Story, 5-Story, 7-Story, and 9-Story SMRFs in Case A and Case D on the soil type B with SSI effects, respectively, subjected to FF record subset. According to the results presented by Fig. 22a–d, SSI effects decreased the seismic failure probability in both performance levels of IO and LS. In the performance level of IO, the seismic failure probability of the 3-Story SMRF in the Case A and Case D decreased by 32.89% (from 0.152 to 0.102) and 60.92% (from 0.238 to 0.145), respectively, and in the performance level of LS, decreased by 22.34% (from 0.564 to 0.438) and 28.03% (from 0.792 to 0.570), respectively. In the performance level of IO, the seismic probability of collapse of the 5-Story SMRF in the Case A and Case D decreased by 22.22% (from 0.09 to 0.07) and 10.92% (from 0.119 to 0.106), respectively, and in the performance level of LS, decreased by 10.49% (from 0.305 to 0.273) and 14.52% (from 0.420 to 0.359), respectively. In the performance level of IO, the seismic probability of collapse of the 7-Story SMRF in the Case A and Case D decreased by 30.55% (from 0.072 to 0.050) and 15.78% (from 0.095 to 0.080), respectively, and in the performance level of LS, decreased by 30.35% (from 0.257 to 0.179) and 27.30% (from 0.315 to 0.229), respectively. In the performance level of IO, the seismic failure probability of the 9-Story SMRF in the Case A and Case D decreased by 14.89% (from 0.047 to 0.040) and 111% (from 0.07 to 0.06), respectively, and in the performance level of LS, decreased by (from 0.172 to 0.141) and 14.28% (from 0.226 to 0.179), respectively. For brevity, the results of SSI effects for soil type B were presented, while similar trends were observed for other soil types and SMRFs.

According to Fig. 22a–d, it can be observed that the $S_a(T_1)$ values in the seismic failure probability of 50% corresponding to the performance levels of IO and LS in Case D were higher than those for Case A considering the SSI effects. Therefore, the results of analysis can be used for SMRFs considering the SSI effects. In addition, in both situation of Case A and Case D, it is shown that the SSI effects increased the seismic failure probability. Therefore, the negative effects of considering SSI should be assumed in modeling process.

5 Conclusions

This research evaluates the seismic performance levels of 3-Story, 5-Story, 7-Story, and 9-Story SMRFs founded on the four soil types assuming four cases of IMWs placement prone to FF subset used by FEMA-P695 (FEMA P695 2009; Yazdanpanah et al. 2022). The results have been focused on the effects of considering IMWs and their significant influence on the fundamental period and seismic responses. To accurately model the IMWs and their effects on the structural response, a Tcl programming algorithm was developed in OpenSees (McKenna et al. 2016) to intelligently control the collapse state of IMWs in each floor level assuming M-IDR of the collapse limit of IMWs equal to 1.75%. It worth noting that, due to considering 2D models, the results of analysis can be used for 2D structures within the context of assumptions. The main remarks can be summarized as follows:

- According to the results of the fundamental period of SMRFs (Table 5), the placement of IMWs can add more stiffness to SMRFs and this can significantly decrease the fundamental periods. For instance, in soil type B, assuming Case D in the 3-Story SMRF can cause the fundamental period to decrease by 18.80% (from 1.17 to 0.95). Therefore, in each soil type, Case D with the full placement of IMWs has a lower fundamental period.

- The $S_a(T_1)$ values in M-IDA curves for the aforementioned SMRFs increased by adding IMWs (i.e. Case B, Case C, and Case D) into the bare frame (i.e. Case A). Therefore, the results confirm that the placement of IMWs in all floor levels increased the lateral resisting strength and this can cause an increase in the seismic performance levels. For soil type B, the $S_a(T_1)$ values in the performance level of TC for the 5-Story SMRF assuming IMWs placement of Case B, Case C, and Case D increased by 41.42%, 29.28%, and 20.18%, respectively.

- The SSI effects on the seismic limit-state capacities of the aforementioned SMRFs have been investigated. The results show that considering the SSI effects significantly decreased the $S_a(T_1)$ values in all performance levels compared to neglecting the SSI effects. For example, assuming SSI effects in the soil type E, the $S_a(T_1)$ values in the performance level of CP for the 5-Story SMRF with IMWs placement of Case B, Case C, and Case D decreased by 37.41% (from 0.751 to 0.470), 29.55% (from 0.758 to 0.534), 24.27% (from 0.828 to 0.627), and 17.44% (from 0.854 to 0.705), respectively. Therefore, it is suggested to consider the SSI effects on the modeling process and seismic vulnerability evaluation.

- Comparing the seismic probability of collapse for the performance levels of IO and LS showed that the $S_a(T_1)$ values corresponding to the seismic collapse probability of 50% for the placement of IMWs in all floor levels (i.e. Case D) are higher than those for the bare frame (i.e. Case A). For brevity, the results of 3-Story SMRF founded on soil type B showed that assuming Case D could increase the seismic collapse probability of the performance levels of IO and LS by 60% and 41.07%, respectively.

- Assuming SSI effects had a reduction influence on the seismic failure probability. Thus, this is important to model SSI and assume its significant influence on the seismic responses. In soil type B and the seismic performance level of LS, assuming SSI effects can decrease the collapse probability of the 5-Story SMRF by 10.49% (from 0.305 to 0.273) and 14.52% (from 0.420 to 0.359), for the Case A and Case D, respectively.

- According to results of analysis presented for SMRFs, IMWs have considerable influence on the fundamental period of SMRFs, which can change the seismic behavior of structures. In addition, the significant effects of IMWs on the seismic performance levels and seismic failure probability cannot be ignored. For future work, three-dimensional modeling of buildings with possibility of out-of-plane failure of IMWs is recommended. In addition, it is suggested to investigate previous damages of IMWs (i.e. in-plane damages), different workmanships and the effects of near-fault seismic records.

Declarations

Conflict of interest The authors declare that there is no conflict of interest, and all authors named in the manuscript are aware of the submission and have agreed for the paper in title of 'Probabilistic assessment of SMRFs with infill masonry walls incorporating nonlinear soil–structure interaction' to be submitted for publication in *Bulletin of Earthquake Engineering*.

References

AISC A (2016). Seismic provisions for structural steel buildings. Chicago, IL: American Institute of Steel Construction. 341–16

Allotey N, El Naggar MH (2008) Generalized dynamic Winkler model for nonlinear soil–structure interaction analysis. Can Geotech J 45(4):560–573

Applied Technology Council, & United States. Federal Emergency Management Agency, (FEMA P695) (2009) Quantification of building seismic performance factors. US Department of Homeland Security, FEMA

ASCE 7-16 (2017) Minimum design loads and associated criteria for buildings and other structures. Reston, VA: American Society of Civil Engineers.

Asgarkhani N, Yakhchalian M, Mohebi B (2020) Evaluation of approximate methods for estimating residual drift demands in BRBFs. Eng Struct 224:110849

Boulanger RW, Curras CJ, Kutter BL, Wilson DW, Abghari A (1999) Seismic soil-pile-structure interaction experiments and analyses. J Geotech Geoenviron Eng 125(9):750–759

Brodsky A, Yankelevsky DZ (2017) Resistance of reinforced concrete frames with masonry infill walls to in-plane gravity loading due to loss of a supporting column. Eng Struct 140:134–150

Buonopane SG, White RN (1999) Pseudodynamic testing of masonry infilled reinforced concrete frame. J Struct Eng 125(6):578–589

Carpine R, Ientile S, Vacca N, Boscato G, Rospars C, Cecchi A, Argoul P (2021) Modal identification in the case of complex modes–Use of the wavelet analysis applied to the after-shock responses of a masonry wall during shear compression tests. Mech Syst Signal Process 160:107753

AISC Committee. (2016). Specification for structural steel buildings (ANSI/AISC 360–16). American Institute of Steel Construction, Chicago-Illinois

Crisafulli FJ, Carr AJ (2007) Proposed macro-model for the analysis of infilled frame structures. Bull N Z Soc Earthq Eng 40(2):69–77

Di Trapani F, Shing PB, Cavaleri L (2018) Macroelement model for in-plane and out-of-plane responses of masonry infills in frame structures. J Struct Eng 144(2):04017198

Dutta SC, Bhattacharya K, Roy R (2004) Response of low-rise buildings under seismic ground excitation incorporating soil–structure interaction. Soil Dyn Earthq Eng 24(12):893–914

El-Dakhakhni WW, Elgaaly M, Hamid AA (2003) Three-strut model for concrete masonry-infilled steel frames. J Struct Eng 129(2):177–185

Elwardany H, Seleemah A, Jankowski R (2017) Seismic pounding behavior of multi-story buildings in series considering the effect of infill panels. Eng Struct 144:139–150

Elwardany H, Seleemah A, Jankowski R, El-Khoriby S (2019) Influence of soil–structure interaction on seismic pounding between steel frame buildings considering the effect of infill panels. Bull Earthq Eng 17(11):6165–6202

Fardis MN, Bousias SN, Franchioni G, Panagiotakos TB (1999) Seismic response and design of RC structures with plan-eccentric masonry infills. Earthq Eng Struct Dyn 28(2):173–191

FEMA-356. (2000) Prestandard and commentary for the seismic rehabilitation of buildings. Washington, DC: Federal Emergency Management Agency.

Forcellini D (2021) Analytical fragility curves of shallow-founded structures subjected to soil-structure interaction (SSI) effects. Soil Dyn Earthq Eng 141:106487

Furtado A, Rodrigues H, Arêde A (2015) Modelling of masonry infill walls participation in the seismic behaviour of RC buildings using OpenSees. Int J Adv Struct Eng (IJASE) 7(2):117–127

Furtado A, Rodrigues H, Arêde A, Varum H (2016a) Experimental evaluation of out-of-plane capacity of masonry infill walls. Eng Struct 111:48–63

Furtado A, Rodrigues H, Arêde A, Varum H (2016b) Simplified macro-model for infill masonry walls considering the out-of-plane behaviour. Earthq Eng Struct Dyn 45(4):507–524

Furtado A, Rodrigues H, Arêde A, Varum H (2017) Modal identification of infill masonry walls with different characteristics. Eng Struct 145:118–134

Furtado A, Rodrigues H, Arêde A (2018) Calibration of a simplified macro-model for infilled frames with openings. Adv Struct Eng 21(2):157–170

Furtado A, Rodrigues H, Arêde A, Varum H (2020) Effect of the panel width support and columns axial load on the infill masonry walls out-of-plane behavior. J Earthq Eng 24(4):653–681

Furtado A, Rodrigues H, Arede A, Varum H (2022) Experimental investigation on the possible effect of previous damage, workmanship and test setup on the out-of-plane behaviour of masonry infill walls. J Earthq Eng 26(11):5647–5678

Furtado A, Rodrigues H, & Arêde A. (2021). Effect of the infill panels in the floor response spectra of an 8-storey RC building. In: structures. Elsevier (Vol 34, pp 2476–2498)

Gara F, Carbonari S, Roia D, Balducci A, Dezi L (2021) Seismic retrofit assessment of a school building through operational modal analysis and fe modeling. J Struct Eng 147(1):04020302

Gazetas G (1991) Formulas and charts for impedances of surface and embedded foundations. J Geotech Eng 117(9):1363–1381

Gupta, A., and Krawinkler, H. (1999). Seismic demands for performance evaluation of steel moment resisting frame structures, technical report 132, The John A. Blume earthquake engineering research Center, department of civil engineering, Stanford University, Stanford, CA.

Harden CW, Hutchinson TC (2009) Beam-on-nonlinear-Winkler-foundation modeling of shallow, rocking-dominated footings. Earthq Spectra 25(2):277–300

Huang X, Zhou Z, Wang Y (2021) Investigation of the seismic behaviour of masonry infilled self-centring beam moment frames using a new infill material model. Bull Earthq Eng 19(12):4887–4910

Ibarra LF, Medina RA, Krawinkler H (2005) Hysteretic models that incorporate strength and stiffness deterioration. Earthq Eng Struct Dyn 34(12):1489–1511

Kakaletsis DJ, Karayannis CG (2008) Influence of masonry strength and openings on infilled R/C frames under cycling loading. J Earthq Eng 12(2):197–221

Karapetrou ST, Fotopoulou SD, Pitilakis KD (2015) Seismic vulnerability assessment of high-rise non-ductile RC buildings considering soil–structure interaction effects. Soil Dyn Earthq Eng 73:42–57

Kazemi F, Mohebi B, Yakhchalian M (2018) Evaluation the P-delta effect on collapse capacity of adjacent structures subjected to far-field ground motions. Civil Eng J 4(5):1066. https://doi.org/10.28991/cej-0309156

Kazemi F, Mohebi B, Yakhchalian M (2020) Predicting the seismic collapse capacity of adjacent structures prone to pounding. Can J Civ Eng 47(6):663–677

Kazemi F, Miari M, Jankowski R (2021a) Investigating the effects of structural pounding on the seismic performance of adjacent RC and steel MRFs. Bull Earthq Eng 19(1):317–343

Kazemi F, Mohebi B, Jankowski R (2021b) Predicting the seismic collapse capacity of adjacent SMRFs retrofitted with fluid viscous dampers in pounding condition. Mech Syst Signal Process 161:107939

Kazemi F, Jankowski R (2023a) Enhancing seismic performance of rigid and semi-rigid connections equipped with SMA bolts incorporating nonlinear soil-structure interaction. Eng Struct 274:114896. https://doi.org/10.1016/j.engstruct.2022.114896

Kazemi F, Jankowski R (2023b) Machine learning-based prediction of seismic limit-state capacity of steel moment-resisting frames considering soil-structure interaction. Comput Struct 274:106886

Kazemi F, Asgarkhani N, Jankowski R (2023) Predicting seismic response of SMRFs founded on different soil types using machine learning techniques. Eng Struct 274:114953

Koutromanos I, Stavridis A, Shing PB, Willam K (2011) Numerical modeling of masonry-infilled RC frames subjected to seismic loads. Comput Struct 89(11–12):1026–1037

Mazza F (2019) In-plane–out-of-plane non-linear model of masonry infills in the seismic analysis of RC-framed buildings. Earthq Eng Struct Dyn 48(4):432–453

Mazza F, Donnici A (2021) In-plane and out-of-plane seismic damage of masonry infills in existing rc structures: the case study of De Gasperi-Battaglia school in Norcia. Bull Earthq Eng 19(1):345–376

McKenna F, Fenves GL, Filippou, FC, & Scott MH (2016) Open system for earthquake engineering simulation (open sees) Berkeley: pacific Earthquake engineering research center, University of California, Web page. http://opensees.berkeley.edu.

Merino RJ, Perrone D, Filiatrault A (2020) Consistent floor response spectra for performance-based seismic design of nonstructural elements. Earthq Eng Struct Dyn 49(3):261–284

Misir IS, Ozcelik O, Girgin SC, Yucel U (2016) The behavior of infill walls in RC frames under combined bidirectional loading. J Earthq Eng 20(4):559–586

Mitropoulou CC, Kostopanagiotis C, Kopanos M, Ioakim D, & Lagaros ND. (2016). Influence of soil–structure interaction on fragility assessment of building structures. In: Structures (Vol 6, pp 85–98).

Mohamed H, Romão X (2020) Analysis of the performance of strut models to simulate the seismic behaviour of masonry infills in partially infilled RC frames. Eng Struct 222:111124

Mohebi B, Yazdanpanah O, Kazemi F, Formisano A (2021) Seismic damage diagnosis in adjacent steel and RC MRFs considering pounding effects through improved wavelet-based damage-sensitive feature. J Build Eng 33:101847

Mohebi B, Kazemi F, Yakhchalian M (2018) Investigating the P-Delta effects on the seismic collapse capacity of adjacent structures. In: 16th European Conference on Earthquake Engineering (16ECEE), 18–21 June, Thessaloniki, Greece

Nicoletti V, Arezzo D, Carbonari S, Gara F (2020) Expeditious methodology for the estimation of infill masonry wall stiffness through in-situ dynamic tests. Constr Build Mater 262:120807

Onat O, Correia AA, Lourenço PB, Koçak A (2018) Assessment of the combined in-plane and out-of-plane behavior of brick infill walls within reinforced concrete frames under seismic loading. Earthq Eng Struct Dyn 47(14):2821–2839

Ozturkoglu O, Ucar T, Yesilce Y (2017) Effect of masonry infill walls with openings on nonlinear response of reinforced concrete frames. Earthq Struct 12(3):333–347

Pecker A, Paolucci R, Chatzigogos C, Correia AA, Figini R (2014) The role of non-linear dynamic soil-foundation interaction on the seismic response of structures. Bull Earthq Eng 12(3):1157–1176

Perrone D, Leone M, Aiello MA (2017) Non-linear behaviour of masonry infilled RC frames: influence of masonry mechanical properties. Eng Struct 150:875–891

Petridis C, Pitilakis D (2020) Fragility curve modifiers for reinforced concrete dual buildings, including nonlinear site effects and soil–structure interaction. Earthq Spectra 36(4):1930–1951

Pitilakis D, Dietz M, Wood DM, Clouteau D, Modaressi A (2008) Numerical simulation of dynamic soil–structure interaction in shaking table testing. Soil Dyn Earthq Eng 28(6):453–467

Pitilakis KD, Karapetrou ST, Fotopoulou SD (2014) Consideration of aging and SSI effects on seismic vulnerability assessment of RC buildings. Bull Earthq Eng 12(4):1755–1776

Preti M, Bettini N, Plizzari G (2012) Infill walls with sliding joints to limit infill-frame seismic interaction: large-scale experimental test. J Earthq Eng 16(1):125–141

Pujol S, Fick D (2010) The test of a full-scale three-story RC structure with masonry infill walls. Eng Struct 32(10):3112–3121

Rajeev P, Tesfamariam S (2012) Seismic fragilities of non-ductile reinforced concrete frames with consideration of soil structure interaction. Soil Dyn Earthq Eng 40:78–86

Ramos LF, Marques L, Lourenço PB, De Roeck G, Campos-Costa A, Roque J (2010) Monitoring historical masonry structures with operational modal analysis: two case studies. Mech Syst Signal Process 24(5):1291–1305

Raychowdhury P (2011) Seismic response of low-rise steel moment-resisting frame (SMRF) buildings incorporating nonlinear soil–structure interaction (SSI). Eng Struct 33(3):958–967

Raychowdhury P, Hutchinson TC (2009) Performance evaluation of a nonlinear Winkler-based shallow foundation model using centrifuge test results. Earthq Eng Struct Dyn 38(5):679–698

Rodrigues H, Varum H, Costa A (2010) Simplified macro-model for infill masonry panels. J Earthq Eng 14(3):390–416

Salmanpour AH, Mojsilović N, Schwartz J (2015) Displacement capacity of contemporary unreinforced masonry walls: an experimental study. Eng Struct 89:1–16

Smyrou E, Blandon C, Antoniou S, Pinho R, Crisafulli F (2011) Implementation and verification of a masonry panel model for nonlinear dynamic analysis of infilled RC frames. Bull Earthq Eng 9(5):1519–1534

Tasnimi AA, Mohebkhah A (2011) Investigation on the behavior of brick-infilled steel frames with openings, experimental and analytical approaches. Eng Struct 33(3):968–980

USGS (2022) US geological survey. http://usgs.gov. Accessed 6 July 2022

Uva G, Porco F, Fiore A (2012) Appraisal of masonry infill walls effect in the seismic response of RC framed buildings: a case study. Eng Struct 34:514–526

Wararuksajja W, Srechai J, Leelataviwat S (2020) Seismic design of RC moment-resisting frames with concrete block infill walls considering local infill-frame interactions. Bull Earthq Eng 18(14):6445–6474

Yakhchalian M, Asgarkhani N, Yakhchalian M (2020) Evaluation of deflection amplification factor for steel buckling restrained braced frames. J Build Eng 30:101228

Yakhchalian M, Yakhchalian M, Asgarkhani N (2021) An advanced intensity measure for residual drift assessment of steel BRB frames. Bull Earthq Eng 19(4):1931–1955

Yazdanpanah O, Mohebi B, Kazemi F, Mansouri I, Jankowski R (2022) Development of fragility curves in adjacent steel moment-resisting frames considering pounding effects through improved wavelet-based refined damage-sensitive feature. Mech Syst Signal Process 173:109038

Zuo H, Zhang W, Wang B, Gu X (2022) Force–displacement relationship modelling of masonry infill walls with openings in hinged steel frames. Bull Earthq Eng 20(1):349–382